Labounek, R., Bondy, M.T., Paulson, A.l., Bédard, S., Abramovic, M., Alonso-Ortiz, E., Atcheson, N.T., Barlow, L.R., Barry, R.L., Barth, M., Battiston, M., Büchel, C., Budde, M.D., Callot, V., Combes, A., De Leener, B., Descoteaux, M., de Sousa, P.L., Dostál, M., Doyon, J., Dvorak, A.V., Eippert, F., Epperson, K.R., Epperson, K.S., Freund, P., Finsterbusch, J., Foias, A., Fratini, M., Fukunaga, I., Gandini Wheeler-Kingshott, C.A.M., Germani, G., Gilbert, G., Giove, F., Grussu, F., Hagiwara, A., Henry, P., Horák, T., Hori, M., Joers, J.M., Kamiya, K., Karbasforoushan, H., Keřkovský, M., Khatibi, A., Kim, J., Kinany, N., Kitzler, H., Kolind, S., Kong, Y., Kudlička, P., Kuntke, P., Kurniawan, N.D., Kusmia, S., Laganà, M.M., Laule, C., Law, C.S.W., Leutritz, T., Liu, Y., Llufriu, S., Mackey, S., Martin, A.R., Martinez-Heras, E., Mattera, L., O'Grady, K.P., Papinutto, N., Papp, D., Pareto, D., Parrish, T.B., Pichiecchio, A., Prados, F., Rovira, A., Ruitenberg, M.J., Samson, R.S., Savini, G., Seif, M., Seifert, A.C., Smith, A.K., Smith, S.A., Smith, Z.A., Solana, E., Suzuki, Y., Tackley, G.W., Tinnermann, A., Valošek, J., Van De Ville, D., Yiannakas, M.C., Weber II, K.A., Weiskopf, N., Wise, R.G., Wyss, P.O., Xu, J., Cohen-Adad, J., Lenglet, C., & Nestrašil, I. (2025). Body size and intracranial volume interact with the structure of the central nervous system: A multi-center in vivo neuroimaging study. *Imaging Neuroscience*, Advance Publication. https://doi.org/10.1162/imag_a_00559

Body size and intracranial volume interact with the structure of the central nervous system: A multi-center in vivo neuroimaging study

René Labounek[1], Monica T. Bondy[1], Amy L. Paulson[1], Sandrine Bédard[2], Mihael Abramovic[3], Eva Alonso-Ortiz[2,4], Nicole T Atcheson[5], Laura R. Barlow[6], Robert L. Barry[7,8,9], Markus Barth[5,10], Marco Battiston[11], Christian Büchel[12], Matthew D. Budde[13,14], Virginie Callot[15,16], Anna Combes[11], Benjamin De Leener[2,4,17], Maxime Descoteaux[18], Paulo Loureiro de Sousa[19], Marek Dostál[20,21], Julien Doyon[22], Adam V. Dvorak[23], Falk Eippert[24], Karla R. Epperson[25], Kevin S. Epperson[25], Patrick Freund[26,27,28], Jürgen Finsterbusch[12], Alexandru Foias[2], Michela Fratini[29,30], Issei Fukunaga[31], Claudia A. M. Gandini Wheeler-Kingshott[11,32], GianCarlo Germani[33], Guillaume Gilbert[34], Federico Giove[30,35], Francesco Grussu[11,36], Akifumi Hagiwara[31], Pierre-Gilles

[1] Division of Clinical Behavioral Neuroscience, Department of Pediatrics, Masonic Institute for the Developing Brain, University of Minnesota, Minneapolis, MN, USA
[2] NeuroPoly Lab, Institute of Biomedical Engineering, Polytechnique Montreal, Montreal, QC, Canada
[3] Department of Radiology, Swiss Paraplegic Centre, Nottwil, Switzerland
[4] Centre de recherche du CHU Sainte-Justine, Université de Montréal, Montreal, QC, Canada
[5] Centre for Advanced Imaging, Australian Institute for Bioengineering and Nanotechnology, The University of Queensland, St Lucia, Australia
[6] Department of Radiology, Faculty of Medicine, University of British Columbia, Vancouver, BC, Canada
[7] Athinoula A. Martinos Center for Biomedical Imaging, Department of Radiology, Massachusetts General Hospital, Charlestown, Massachusetts, USA
[8] Harvard Medical School, Boston, Massachusetts, USA
[9] Harvard-Massachusetts Institute of Technology Health Sciences & Technology, Cambridge, Massachusetts, USA
[10] School of Electrical Engineering and Computer Science, The University of Queensland, St Lucia, Australia
[11] NMR Research Unit, Queen Square Multiple Sclerosis Centre, Department of Neuroinflammation, Queen Square Institute of Neurology, Faculty of Brain Sciences, University College London, UK
[12] Department for Systems Neuroscience, University Medical Center Hamburg-Eppendorf, Hamburg, Germany
[13] Department of Neurosurgery, Medical College of Wisconsin, Milwaukee, WI, USA
[14] Clement J. Zablocki Veteran's Affairs Medical Center, Milwaukee, WI, USA
[15] Aix-Marseille Univ, CNRS, CRMBM, Marseille, France
[16] APHM, Hopital Universitaire Timone, CEMEREM, Marseille, France
[17] Department of Computer Engineering and Software Engineering, Polytechnique Montreal, Montreal, QC, Canada
[18] Sherbrooke Connectivity Imaging Lab (SCIL), Computer Science department, Université de Sherbrooke, Sherbrooke, QC, Canada
[19] Université de Strasbourg, CNRS, ICube, Strasbourg, France
[20] Department of Radiology and Nuclear Medicine, University Hospital Brno and Masaryk University, Czech Republic
[21] Department of Biophysics, Faculty of Medicine, Masaryk University, Brno, Czech Republic
[22] McConnell Brain Imaging Centre, Montreal Neurological Institute, McGill University, Montreal, Quebec, Canada
[23] Department of Physics and Astronomy, University of British Columbia, Vancouver, BC, Canada
[24] Max Planck Research Group Pain Perception, Max Planck Institute for Human Cognitive and Brain Sciences, Leipzig, Germany
[25] Stanford University, Stanford, CA, USA
[26] Spinal Cord Injury Center Balgrist, University Hospital Zurich, University of Zurich, Zurich, Switzerland
[27] Wellcome Trust Centre for Neuroimaging, Queen Square Institute of Neurology, University College London, London, UK
[28] Department of Neurophysics, Max Planck Institute for Human Cognitive and Brain Sciences, Stephanstraße 1a, 04103 Leipzig, Germany
[29] Institute of Nanotechnology, CNR, Rome, Italy
[30] IRCCS Santa Lucia Foundation, Neuroimaging Laboratory, Rome, Italy
[31] Department of Radiology, Juntendo University School of Medicine, 1-2-1, Hongo, Bunkyo, Tokyo 113-8421, Japan
[32] Department of Brain and Behavioural Sciences, University of Pavia, Pavia, Italy
[33] Advanced Imaging and Artificial Intelligence Center, Neuroradiology Department, IRCCS Mondino Foundation, Pavia, Italy
[34] MR Clinical Science, Philips Healthcare Canada, Mississauga, Canada
[35] CREF - Museo storico della fisica e Centro studi e ricerche Enrico Fermi, Rome, Italy
[36] Vall d'Hebron Institute of Oncology (VHIO), Vall d'Hebron Barcelona Hospital Campus, Barcelona, Spain

Henry[37], Tomáš Horák[38,39,40], Masaaki Hori[31,41], James M. Joers[37], Kouhei Kamiya[41], Haleh Karbasforoushan[42], Miloš Keřkovský[20], Ali Khatibi[43,44,45], Joo-won Kim[46,47,48], Nawal Kinany[49,50], Hagen Kitzler[51], Shannon Kolind[6,23,52], Yazhuo Kong[53,54], Petr Kudlička[40,55], Paul Kuntke[51], Nyoman D. Kurniawan[5], Slawomir Kusmia[56], Maria Marcella Laganà[57], Cornelia Laule[6,23,58,59], Christine S. W. Law[25], Tobias Leutritz[28], Yaou Liu[60], Sara Llufriu[61], Sean Mackey[62], Allan R. Martin[63], Eloy Martinez-Heras[61,64], Loan Mattera[65], Kristin P. O'Grady[66,67], Nico Papinutto[42], Daniel Papp[2,68], Deborah Pareto[64], Todd B. Parrish[69], Anna Pichiecchio[32,33], Ferran Prados[11,70,71], Àlex Rovira[64], Marc J. Ruitenberg[72], Rebecca S. Samson[11], Giovanni Savini[73,74], Maryam Seif[26,28], Alan C. Seifert[46], Alex K. Smith[68], Seth A. Smith[66,67,75], Zachary A. Smith[76], Elisabeth Solana[61], Yuichi Suzuki[77],

[37] Center for Magnetic Resonance Research, Department of Radiology, University of Minnesota, Minneapolis, MN, USA
[38] Faculty of Medicine, Masaryk University, Brno, Czech Republic
[39] Department of Neurology, University Hospital Brno, Brno, Czech Republic
[40] Multimodal and Functional Imaging Laboratory, Central European Institute of Technology, Brno, Czech Republic
[41] Department of Radiology, Toho University Omori Medical Center, Tokyo, Japan
[42] Department of Neurology, UCSF Weill Institute for Neurosciences, University of California San Francisco, San Francisco, CA, USA
[43] Centre of Precision Rehabilitation for Spinal Pain (CPR Spine), University of Birmingham, Birmingham, UK
[44] Centre for Human Brain Health, University of Birmingham, Birmingham, UK
[45] Institute for Mental Health, University of Birmingham, Birmingham, UK
[46] Biomedical Engineering and Imaging Institute, Department of Radiology, Graduate School of Biomedical Sciences, Icahn School of Medicine at Mount Sinai, New York, USA
[47] Department of Radiology, Baylor College of Medicine, Houston, Texas, USA
[48] Department of Psychiatry, Baylor College of Medicine, Houston, Texas, USA
[49] Neuro-X Institute, Ecole polytechnique fédérale de Lausanne, Geneva, Switzerland
[50] Department of Radiology and Medical Informatics, Faculty of Medicine, University of Geneva, Switzerland
[51] Institute of Diagnostic and Interventional Neuroradiology, Faculty of Medicine and Carl Gustav Carus University Hospital, Technische Universität Dresden, Germany
[52] Division of Neurology, Faculty of Medicine, University of British Columbia, Vancouver, BC, Canada
[53] CAS Key Laboratory of Behavioral Science, Institute of Psychology, Chinese Academy of Science, Beijing, 100101, China
[54] Department of Psychology, University of Chinese Academy of Sciences, Beijing, 100049, China
[55] First Department of Neurology, St. Anne's University Hospital and Medical Faculty of Masaryk University, Brno, Czech Republic
[56] IBM Poland, Department of Content Design, Cracow, Poland
[57] Canon Medical Systems srl, Rome, Italy
[58] Department of Pathology & Laboratory Medicine, University of British Columbia, Vancouver, Canada
[59] International Collaboration on Repair Discoveries (ICORD), University of British Columbia, Vancouver, Canada
[60] Department of Radiology, Beijing Tiantan Hospital, Capital Medical University, China
[61] Neuroimmunology and Multiple Sclerosis Unit, Laboratory of Advanced Imaging in Neuroimmunological Diseases (ImaginEM), Hospital Clinic Barcelona, Fundació de Recerca Clínic Barcelona-IDIBAPS and Universitat de Barcelona. Barcelona, Spain
[62] Division of Pain Medicine, Department of Anesthesiology, Perioperative and Pain Medicine, Stanford University School of Medicine, Palo Alto, CA, USA
[63] Department of Neurological Surgery, University of California, Davis, CA, USA
[64] Section of Neuroradiology, Department of Radiology, Hospital Universitari Vall d'Hebron, Barcelona, Spain
[65] Fondation Campus Biotech Geneva, Genève, Switzerland
[66] Vanderbilt University Institute of Imaging Science, Vanderbilt University Medical Center, Nashville, TN, USA
[67] Department of Radiology and Radiological Sciences, Vanderbilt University Medical Center, Nashville, TN, USA
[68] Wellcome Centre For Integrative Neuroimaging, FMRIB, Nuffield Department of Clinical Neurosciences, University of Oxford, Oxford, UK
[69] Department of Radiology, Northwestern University, Chicago, IL 60611, USA
[70] e-Health Center, Universitat Oberta de Catalunya, Barcelona, Spain
[71] Centre for Medical Image Computing, University College London, London, UK
[72] School of Biomedical Sciences, Faculty of Medicine, The University of Queensland, St Lucia, Australia
[73] Department of Biomedical Sciences, Humanitas University, Via Rita Levi Montalcini 4, 20072, Pieve Emanuele (MI), Italy
[74] Neuroradiology Unit, IRCCS Humanitas Research Hospital, Via Alessandro Manzoni 56, 20089, Rozzano (MI), Italy
[75] Department of Biomedical Engineering, Vanderbilt University, Nashville, TN USA
[76] Department of Neurosurgery, University of Oklahoma, Oklahoma City, OK, USA
[77] The University of Tokyo Hospital, Radiology Center, Tokyo, Japan

George W Tackley[78], Alexandra Tinnermann[12], Jan Valošek[2,79,80,81], Dimitri Van De Ville[49,50], Marios C. Yiannakas[11], Kenneth A. Weber II[62], Nikolaus Weiskopf[27,28,82], Richard G. Wise[78,83,84], Patrik O. Wyss[3], Junqian Xu[46,47,48], Julien Cohen-Adad[2,4,79,85,], Christophe Lenglet[37], Igor Nestrašil[1,37]

Senior authors:
Julien Cohen-Adad, Christophe Lenglet and Igor Nestrašil contributed equally to this work.

Corresponding author:
René Labounek, email: rlaboune@umn.edu, Masonic Institute for the Developing Brain, 2025 E River Pkwy, office 2-359, Minneapolis, MN 55414, USA

Keywords
spinal cord, brain, body height and weight, intracranial volume, structural magnetic resonance imaging, in vivo human neuroimaging

Abstract
Clinical research emphasizes the implementation of rigorous and reproducible study designs that rely on between-group matching or controlling for sources of biological variation such as subject's sex and age. However, corrections for body size (i.e. height and weight) are mostly lacking in clinical neuroimaging designs. This study investigates the importance of body size parameters in their relationship with spinal cord (SC) and brain magnetic resonance imaging (MRI) metrics. Data were derived from a cosmopolitan population of 267 healthy human adults (age 30.1±6.6 years old, 125 females). We show that body height correlates with brain gray matter (GM) volume, cortical GM volume, total cerebellar volume, brainstem volume, and cross-sectional area (CSA) of cervical SC white matter (CSA-WM; $0.44 \leq r \leq 0.62$). Intracranial volume (ICV) correlates with body height ($r=0.46$) and the brain volumes and CSA-WM ($0.37 \leq r \leq 0.77$). In comparison, age correlates with cortical GM volume, precentral GM volume, and cortical thickness ($-0.21 \geq r \geq -0.27$). Body weight correlates with magnetization transfer ratio in the SC WM, dorsal columns, and lateral corticospinal tracts ($-0.20 \geq r \geq -0.23$). Body weight further correlates with the mean diffusivity derived from diffusion tensor imaging (DTI) in SC WM ($r=-0.20$) and dorsal columns (-0.21), but only in males. CSA-WM correlates with brain volumes ($0.39 \leq r \leq 0.64$), and with precentral gyrus thickness and DTI-based fractional anisotropy in SC dorsal columns and SC lateral corticospinal tracts ($-0.22 \geq r \geq -0.25$). Linear mixture of age, sex, or sex and age, explained 2±2%, 24±10%, or 26±10%, of data variance in brain volumetry and SC CSA. The amount of explained variance increased to 33±11%, 41±17%, or 46±17%, when body height, ICV, or body height and ICV, were added into the mixture model. In females, the explained variances halved suggesting another unidentified biological factor(s) determining females' CNS morphology. In conclusion, body size and ICV are significant biological variables. Along with sex and age, body size should therefore be included as a mandatory variable in the design of clinical neuroimaging studies examining SC and brain structure; and body size and ICV should be considered as covariates in statistical analyses. Normalization of different brain regions with ICV diminishes their correlations with body size, but simultaneously amplifies ICV-related variance ($r=0.72 \pm 0.07$) and suppresses volume variance of the different brain regions ($r=0.12 \pm 0.19$) in the normalized measurements.

[78] Cardiff University Brain Research Imaging Centre (CUBRIC), School of Psychology, Cardiff University, Cardiff, Wales, UK
[79] Mila - Quebec AI Institute, Montreal, QC, Canada
[80] Department of Neurosurgery, Faculty of Medicine and Dentistry, Palacký University Olomouc, Olomouc, Czech Republic
[81] Department of Neurology, Faculty of Medicine and Dentistry, Palacký University Olomouc, Olomouc, Czech Republic
[82] Felix Bloch Institute for Solid State Physics, Faculty of Physics and Earth Sciences, Leipzig University, Linnéstraße 5, 04103 Leipzig, Germany
[83] Department of Neurosciences, Imaging, and Clinical Sciences, 'G. D'Annunzio' University of Chieti-Pescara, Chieti, Italy
[84] Institute for Advanced Biomedical Technologies, 'G. D'Annunzio' University of Chieti-Pescara, Chieti, Italy
[85] Functional Neuroimaging Unit, CRIUGM, University of Montreal, Montreal, Canada

1 Introduction

Knowledge about the relationship between body size (i.e., height and weight), spinal cord (SC) and brain structure is essential for a mechanistic understanding of human physiology and pathophysiology and, consequently, developing biomarkers critical for robust clinical trial designs. Besides sex and age, numerous other factors influence body size, including genetic makeup, race and ethnicity, socioeconomic and environmental factors, as well as developmental determinants. There are also diseases affecting physical makeup, spanning chronic conditions (i.e., anemia, asthma, celiac disease, inflammatory bowel disease, kidney or heart insufficiency), hormonal diseases (i.e., growth or thyroid hormone disbalances), and/or rare disorders such as achondroplasia and Down, Noonan or Turner syndromes (Butler et al., 2022; Pierpont et al., 2024). For example, patients diagnosed with Friedreich ataxia tend to be underweight in young age and overweight in adulthood (Boesch & Indelicato, 2021; M. Patel et al., 2021). Patients with different types of mucopolysaccharidoses are known to present with a short stature (Lin et al., 2019; Muschol et al., 2019; P. Patel et al., 2014). While neuroimaging measurements are usually compared to a healthy population, neither body height nor weight have been rigorously considered as putative confounding factors, normalization factors, and/or as variables necessary for an inter-population matching (Harding et al., 2021; Joers et al., 2022; Kovac et al., 2022; Provenzale et al., 2015; Rezende et al., 2023; Yund et al., 2015). Such a study design deficit can lead to bias in clinical outcomes, which applies even more explicitly to studies where the typical body size of the patients' cohort differs from the control group. To assess the significance and importance of body size correction, we have investigated the impact of body size on structural neuroimaging measurements in the SC and brain of a healthy human population. *If the effect is significant, future clinical research studies and trials utilizing neuroimaging should include body size as a potential confounding biological factor to avoid bias in clinical outcomes.*

Evolutionary biology has identified links between species' body weight, SC, and cerebral weights (MacLarnon, 1996b), and between spinal canal dimensions and adjacent cord (MacLarnon, 1995, 1996a). Cadaveric human measurements revealed links between the cross-sectional area (CSA) of the cervical SC and cerebral weight, body height, and age (Kameyama et al., 1994). However, in vivo evidence of such a relationship between body size and central nervous system (CNS) structure is limited to a few magnetic resonance imaging (MRI) studies. In vivo CSA of the upper cervical SC (i.e., C2/3 segment) appears to be determined by both the cerebral volume and white matter (WM) content of cerebrospinal tracts (Engl et al., 2013). Recent exploration of the UK Biobank imaging dataset observed weak in vivo links between the CSA of the C2/3 SC segment and body height and weight, and moderate links between the CSA and brain and thalamus volumes (Alfaro-Almagro et al., 2018; Bédard & Cohen-Adad, 2022; Littlejohns et al., 2020). Weak correlations between body height, CSA of the SC (CSA-SC) and gray matter (GM) as well as brain volume scaling were also reported on a concurrent in vivo dataset (Papinutto et al., 2020). However, these effects disappeared when sex was controlled for (Papinutto et al., 2020). Additionally, the in vivo CSA of peripheral nerves has also been shown to correlate moderately with body height, body weight, and body mass index (BMI), but not age (Kronlage et al., 2019). Whether SC WM and GM contents are equally correlated with body size and distinct brain morphology has not been satisfactorily determined. Our **first hypothesis** was therefore that *"CSA of cervical SC WM and GM interacts with body size and morphology of distinct brain structures"*; we tested this premise by utilizing a multi-center *spine-generic* MRI dataset. The dataset allows for the separate assessment of cervical SC WM and GM morphology in a large cohort of healthy cosmopolitan volunteers with available demographic records and images of cerebral morphology (Cohen-Adad et al., 2021a, 2021b).

Myelin content is an essential characteristic of the neural tissue microstructural integrity (Levitan & Kaczmarek, 2002). In the CNS, the ratio between axon diameter and diameter of the total nerve fiber (axon and myelin) is 0.6–0.7 (Susuki, 2010). As SC axons generally have larger diameters than axons within the brain (Aboitiz et al., 1992; Duval et al., 2019; Saliani et al., 2017; Veraart et al., 2020), SC myelin sheaths are often also thicker, increasing the overall diameter of the myelinated axons. Thicker myelin sheaths around axons accelerate

nerve conduction speed independent of the axonal diameter (Rushton, 1951; Zalc, 2006, 2016). Assuming a fairly constant axon/fiber diameter ratio (Susuki, 2010), thicker myelin sheaths are therefore expected for species with larger body sizes (Zalc, 2006, 2016). Considering intra-species variability in body size, the overall degree of SC myelination might be influenced by the body size of a given specimen. If true, the influence of body size on myelin content may be detectable in SC images sensitive to tissue microstructure, such as diffusion tensor imaging (DTI) or magnetization transfer ratio (MTR) imaging. Both DTI and MTR image contrasts are available within the *spine-generic* dataset (Cohen-Adad et al., 2021a, 2021b). Moreover, body weight and BMI are correlated with MTR of peripheral nerves and muscles (Fösleitner et al., 2022). Our **second hypothesis** was therefore that *"SC microstructure, as measured using MTR and DTI, interacts with body size"*.

Finally, the human brain volume and CSA-SC differ between sexes (Bédard & Cohen-Adad, 2022; Giedd et al., 1996; Papinutto et al., 2015, 2020). It is well established that brain volume shrinks and cortical GM thickness thins with aging (Fjell et al., 2013; Peters, 2006; Thambisetty et al., 2010), with both processes accelerating after 45 years of age (Heymsfield et al., 2009; Peters, 2006). However, results obtained from pathological (Callaghan et al., 2014; Kameyama et al., 1994; Weitzenkamp et al., 2001; Zhang et al., 1996; Zhou et al., 1996) and neuroimaging (Callaghan et al., 2014) studies investigating the relationships between age and SC CSA have been less consistent. Recent high-resolution in vivo neuroimaging indeed observed weaker and slower aging effects in SC CSA than those described for brain morphology (Bédard & Cohen-Adad, 2022; Papinutto et al., 2015, 2020). The UK Biobank dataset already showed that physical measures, including body height and weight, strongly impact quantitative brain structural measures in a population of 40-69 years olds while adjusted for sex and age (Miller et al., 2016). Outside of the UK Biobank, links between body size and brain volume have been reported with inconsistent results, spanning significant relationships with a stronger height influence (Baaré et al., 2001; Bédard & Cohen-Adad, 2022; Heymsfield et al., 2009) or non-significant findings (Willerman et al., 1991). Therefore, our **third hypothesis** was that: *"Cerebral morphology interacts with body height more profoundly than with body weight and age."*

In addition to body size, brain morphology is often normalized with subject-specific intracranial volume (ICV) (Voevodskaya et al., 2014; Whitwell et al., 2001; Xie et al., 2005). ICV and head size were identified as significant covariates determining brain structure more profoundly than the body size in the UK Biobank dataset (Miller et al., 2016). That led us to the **fourth hypothesis**: *"Body size increases the predictive power of CNS structure."* We tested our hypotheses by utilizing the *spine-generic* dataset of predominantly non-elderly healthy adults and considering sex effects.

2 Methods

2.1 Structural MRI data

Signed informed consent was obtained from all participants under the compliance of the corresponding local ethics committee (more info in the *Scientific Data* paper (Cohen-Adad et al., 2021b)). The *spine-generic* protocol 3T MRI data were acquired once for each participant. Siemens scanners were used in 180 (67.41%) acquisitions, Philips scanners in 50 (18.72%) acquisitions and GE scanners in 37 (13.87%) acquisitions. 3D T1w scans were utilized to estimate cerebral volumes and cortical thicknesses. 3D T2w scans were utilized to assess the cross-sectional area (CSA) of the cervical spinal cord (SC). Axial T2*w scans were utilized to estimate the CSA of white (WM) and gray (GM) matter of the cervical SC. Diffusion weighted imaging was utilized to estimate diffusion tensor imaging (DTI) and the corresponding microstructural maps for the cervical SC. GRE-T1w, GRE-MT1, and GRE-MT0 scans were used to derive the magnetization transfer ratio (MTR) maps in the cervical SC. More detailed information about protocol settings and scanner subtypes can be found in the *spine-generic* protocol original papers (Cohen-Adad et al., 2021a, 2021b).

2.2 Image analysis

The same image processing pipeline was employed here, utilizing the Spinal Cord Toolbox (SCT) version 6.1 (De Leener et al., 2017), as developed originally for the *spine-generic* protocol (Cohen-Adad et al., 2021a, 2021b). The *spine-generic* database (Cohen-Adad et al., 2021b) includes manual SC and/or WM/GM segmentation and cervical level labeling for MRI scans where the automated segmentation and/or labeling methods were inaccurate. In cases where manual segmentation existed, we used the existing manual segmentation to secure result reproducibility and reliability. CSA of the whole SC (CSA-SC) was computed and averaged from cervical C3-4 vertebral levels of the 3D T2w scan. CSA of WM and GM structures (CSA-WM, CSA-GM) were computed and averaged from cervical C3-4 levels of the axial T2*w scan. C3-4 levels were selected for CSA measurements since the T2*w imaging protocol had set the center of the field of view at the C3/4 disc and because C3-4 levels still contain the most sensory and motor fiber bundles. C3-4 average represents a robust representative morphological measurement as the CSA demonstrates high intra-individual correlation over segments (Healy et al., 2012; Kameyama et al., 1996), although the absolute CSA values inter-individually vary (Cohen-Adad et al., 2021b). All CSA measurements were measured in mm^2 units. FA, MD, RD, and MTR were estimated from cervical C2-5 vertebral levels for WM, GM, bilateral lateral corticospinal tracts, and bilateral dorsal columns utilizing the PAM50 atlas co-registration and weighted average techniques (Lévy et al., 2015). The C2-5 segment range was selected for DTI and MTR averaging to guarantee the robustness of the tract-specific measurements with minimal partial volume effects (Lévy et al., 2015).

Brain volume was segmented and parceled at partial sub-structures from 3D T1w scans with FreeSurfer ver. 7.2 (Fischl, 2012). All FreeSurfer-based brain imaging results were visually reviewed for accuracy and any inaccurate segmentations were fixed. During initial post-processing, 112 scans (46.86%) had inaccurate segmentation. Corrections were performed using FreeSurfer edits (i.e., control points, pial edits, both control points and pial edits, and recon-all interventions), AFNI's (Analysis of Functional NeuroImages) 3dUnifize tool (Cox, 1996), and/or lesion fill using ITK-SNAP (Yushkevich et al., 2006) and FSL (Battaglini et al., 2012; Jenkinson et al., 2012). The lesion fill was utilized for 1 scan *(sub-mountSinai01*) where minor white matter hypo-intensities were present. Volumes of brain (BrainVol), brain GM (BrainGMVol), cortical GM (CorticalGMVol), cortical WM (CorticalWMVol), subcortical GM (SubCortGMVol, including amygdala, caudate, hippocampus, nucleus accumbens, pallidum, putamen, thalamus, ventral diencephalon, and substancia nigra), thalamus (ThalamusVol), cerebellum (CerebellumVol), brainstem (BrainStemVol), precentral cortex GM (PrecentralGMVol), postcentral cortex GM (PostcentralGMVol), and intracranial volume (ICV) were measured from the FreeSurfer segmentations in mm^3 units. A sub-analysis also utilized brain volume measurements as relative ratios of the whole ICV. Cortical thickness (Cortical thickness), thickness of the precentral (PrecentralG Thickness), and postcentral gyrus (PostcentralG Thickness) were averaged across the left and right hemispheres as derived from the surface-based cortical parcellation. Precentral and postcentral cortices, motor and somatosensory cerebral centers, were investigated because the majority of the cervical spinal cord WM cross-section are the motor and somatosensory pathways.

2.3 Exclusion of spinal cord and brain structural measurements

Spinal cord images were analyzed for all 267 participants. Cross-sectional area of SC (CSA-SC) was not estimated for 4 participants (listed in the category "csa_t2" in exclude.yml file, which contains the excluded subject ID and the verbal explanation of the exclusion; 1.50% of the dataset), CSA of WM and GM (CSA-WM and CSA-GM respectively) were not estimated for 4 different participants (category "csa_gm" in the exclude.yml file; 1.50%), DTI measurements were not estimated for 4 participants (categories "dti_fa", "dti_md" and "dti_rd" in the exclude.yml file; 1.50%), and MTR measurements were not estimated for 5 participants (category "mtr" in the exclude.yml file; 1.87%). The exclude.yml file is available at: https://github.com/spine-generic/data-multi-subject/blob/r20231212/exclude.yml. The most common reasons for SC measurement exclusions were: (*i*) motion artifacts; (*ii*) subject repositioning during data acquisition; (*iii*) poor data quality; (*iv*) wrong field of view placement; or (*v*) not following required imaging parameters. The

analysis excluded all CSA, DTI and MTR SC measurements for 1 additional subject (*sub-mniS05*; 0.37% of the dataset) due to severe degenerative cervical SC compression (maximal compression at C3/C4 level).

We analyzed brain images from 239 participants (89.51% of the dataset). We excluded T1w scans of 28 participants (10.49%) from the analysis because the images demonstrated field of view cut-offs (18 scans; 6.74%), defacing errors (5 scans; 1.87%), poor image contrast in superior cerebral regions (4 scans; 1.50%), and severe motion artifacts (1 scan; 0.37%). Excluded brain scans are listed in the exclude.yml file as the category “brain_t1”.

2.4 Body mass measurements

Body mass index (Nuttall, 2015), body surface area (Du Bois & Du Bois, 1989) and lean body weight (James, 1976) were estimated utilizing body height and weight measurements.

2.5 Effect of ICV normalization on cross-sectional brain volume measurements

Let x be a region-specific brain volume measurement. If $x \ll$ ICV (e.g., ThalamusVol), then a normalized brain volume $x_{norm}=x/ICV$ becomes proportional to ICV^{-1} and an effect of the underlying region-specific brain structure can be minimized in the normalized volume measurement. In the statistical analysis, we correlated x_{norm} with original x [mm^3] and ICV^{-1} to test whether x_{norm} preserves more information about x or ICV. We also correlated x and x_{norm} with body size and assessed outcome differences.

2.6 Statistical analysis

Statistical analysis and figure visualization were implemented in the programming environment MATLAB R2021b (*Natick, USA*). Each variable or log(variable) was normalized into the space of the normal distribution and the Kruskall-Wallis test tested whether investigated variables meet conditions for Gaussian or log-Gaussian distribution ($p<0.05$). Between-group differences were tested with two-sample or paired t-tests. Correlation analysis utilized Pearson (r) and Spearman (ρ) correlation coefficients, considering correlation to be significant if $p_{FWE}<0.05$ (FWE - family wise error correction) after the Bonferroni multiple-comparison correction. Correlation coefficients were estimated for raw and normalized dataset values, where the manufacturer-specific average was subtracted from all SC quantitative measurements to minimize the effects of the previously reported inter-manufacturer variability in the spine-generic dataset (Cohen-Adad et al., 2021b). For SC DTI and MTR correlation analysis, GE scanner raw values were excluded (i.e., 13.87% of the dataset) due to strong offsets compared to Siemens and Philips scanner values. SC qMRI measurements, FreeSurfer-based brain measurements, age, body height, and body weight were cross-correlated, and significant correlations (after the Bonferroni correction) were identified. The dataset was split into males and females and the correlation analysis was post-hoc repeated to address sex effects in the data demonstrating significant correlations. Due to the reduced sample size at half, the uncorrected $p<0.05$ was considered significant in the post-hoc analysis investigating the sex effects. The correlation analysis was also post-hoc repeated for SC measurements while excluding all 64 subjects with degenerative cervical SC compression (as identified in the *spine-generic* database; r20231212) to test for the compression effects on the study outcomes. The critical $p_{FWE}<0.05$ remained here, although the dataset was reduced to 76% of its original size.

Manufacturer-specific average was subtracted from all SC structural measurements. Then, all multivariate data were normalized to mean=0 and standard deviation STD=1 for each examined variable. Such normalized data formed an input matrix for exploratory principal component analysis (PCA) optimized via singular value decomposition. Variables were visualized in the space of orthogonal principal components via biplot projections, and between-variable relationships were quantified and interpreted in the rotated principal space explaining the majority of the data variance.

Several linear regression models (Eqs. 1-10) were estimated for the SC and brain structural measurements ($\boldsymbol{y}$) demonstrating significant correlation with age, ICV, body height and/or body weight, respectively. Models’ coefficients of determination (R^2) objectively assessed which demographic variable or set of demographic

variables explained most of the demography-related variance in the SC and brain structure. Models utilizing simultaneous regression of body height and body weight were not utilized as body height and weight are strongly linearly dependent variables. The variable $\boldsymbol{y_0}$ represents the model's constant member, the β parameters are model regression coefficients (Eqs. 1-14). Categorical variable ***Sex*** was modeled as a vector of values 0.5 at positions of males and of values -0.5 at positions of females. Manufacturer-specific average was subtracted from all SC structural measurements before the regression analysis.

$$\boldsymbol{y} \propto \boldsymbol{y}_0 + \beta_{Age} \cdot \boldsymbol{Age} \quad (1)$$

$$\boldsymbol{y} \propto \boldsymbol{y}_0 + \beta_{Sex} \cdot \boldsymbol{Sex} \quad (2)$$

$$\boldsymbol{y} \propto \boldsymbol{y}_0 + \beta_{Height} \cdot \boldsymbol{Height} \quad (3)$$

$$\boldsymbol{y} \propto \boldsymbol{y}_0 + \beta_{Weight} \cdot \boldsymbol{Weight} \quad (4)$$

$$\boldsymbol{y} \propto \boldsymbol{y}_0 + \beta_{ICV} \cdot \boldsymbol{ICV} \quad (5)$$

$$\boldsymbol{y} \propto \boldsymbol{y}_0 + \beta_{Sex} \cdot \boldsymbol{Sex} + \beta_{Age} \cdot \boldsymbol{Age} \quad (6)$$

$$\boldsymbol{y} \propto \boldsymbol{y}_0 + \beta_{Sex} \cdot \boldsymbol{Sex} + \beta_{Height} \cdot \boldsymbol{Height} \quad (7)$$

$$\boldsymbol{y} \propto \boldsymbol{y}_0 + \beta_{Sex} \cdot \boldsymbol{Sex} + \beta_{Weight} \cdot \boldsymbol{Weight} \quad (8)$$

$$\boldsymbol{y} \propto \boldsymbol{y}_0 + \beta_{Sex} \cdot \boldsymbol{Sex} + \beta_{ICV} \cdot \boldsymbol{ICV} \quad (9)$$

$$\boldsymbol{y} \propto \boldsymbol{y}_0 + \beta_{Sex} \cdot \boldsymbol{Sex} + \beta_{Age} \cdot \boldsymbol{Age} + \beta_{Height} \cdot \boldsymbol{Height} \quad (10)$$

$$\boldsymbol{y} \propto \boldsymbol{y}_0 + \beta_{Sex} \cdot \boldsymbol{Sex} + \beta_{Age} \cdot \boldsymbol{Age} + \beta_{Weight} \cdot \boldsymbol{Weight} \quad (11)$$

$$\boldsymbol{y} \propto \boldsymbol{y}_0 + \beta_{Sex} \cdot \boldsymbol{Sex} + \beta_{Age} \cdot \boldsymbol{Age} + \beta_{ICV} \cdot \boldsymbol{ICV} \quad (12)$$

$$\boldsymbol{y} \propto \boldsymbol{y}_0 + \beta_{Sex} \cdot \boldsymbol{Sex} + \beta_{Age} \cdot \boldsymbol{Age} + \beta_{ICV} \cdot \boldsymbol{ICV} + \beta_{Height} \cdot \boldsymbol{Height} \quad (13)$$

$$\boldsymbol{y} \propto \boldsymbol{y}_0 + \beta_{Sex} \cdot \boldsymbol{Sex} + \beta_{Age} \cdot \boldsymbol{Age} + \beta_{ICV} \cdot \boldsymbol{ICV} + \beta_{Weight} \cdot \boldsymbol{Weight} \quad (14)$$

Stepwise linear regression was also performed utilizing the same variables as in the Eqs. 1-14. The threshold p-value to consider a variable as statistically significant for the multiple linear regression model was $p<0.05$.

3 Results

3.1 Study cohort demography

Structural MRI data were acquired in a cohort of 267 neurologically healthy (self-reported) volunteers whose demographic data and intracranial volumes are summarized in **Table 1**. There was no significant difference in age between females and males, but body height, weight, BMI, body surface area (BSA), lean body weight (LBW) and ICV differed (**Table 1**). Female dataset provided slightly lower variance in age, body height, body weight, BSA, LBW and ICV; and slightly higher variance in BMI (**Table 1**). All subject-specific demographic data are available at: https://github.com/spine-generic/data-multi-subject/blob/r20231212/participants.tsv. Body height and weight were significantly intercorrelated (Pearson correlation coefficient r=0.702). ICV correlated significantly with body height (r=0.463) and weight (0.357). However, the correlation coefficient magnitudes shows that ICV and body size were also carrying portions of mutually independent information. Moreover, only correlation between ICV and body height in males survived significance when the dataset was split regarding the sex (**Table 2**).

	All	Female	Male	p-value
Number of subjects	267	125 (46.82%)	142 (53.18%)	
Age [years]	30.1±6.6 (19.0-56.0)	29.4±6.4 (20.0-56.0)	30.6±6.7 (19.0-56.0)	0.1537
Height [cm]	172.1±10.0 (148.0-203.0)	164.9±6.5 (148.0-185.0)	178.5±8.0 (161.0-203.0)	<0.0001
Weight [kg]	68.3±13.4 (41.0-120.0)	59.5±9.7 (41.0-86.0)	76.0±11.4 (55.0-120.0)	<0.0001
BMI [kg/m^2]	22.9±3.3 (16.6-35.5)	21.9±3.5 (16.6-35.5)	23.8±2.8 (18.6-35.1)	<0.0001
BSA [m^2]	1.80±0.21 (1.35-2.42)	1.65±0.13 (1.35-2.01)	1.94±0.17 (1.60-2.42)	<0.0001
LBW [kg]	52.5±10.0 (33.5-78.1)	44.0±4.5 (33.5-56.0)	60.2±6.8 (46.2-78.1)	<0.0001
ICV [*10^{6}mm^3]	1.48±0.23 (0.95-2.10)	1.34±0.18 (0.95-1.72)	1.59±0.20 (0.99-2.10)	<0.0001

Table 1: Demography and intracranial volume of recruited cohort.
Cell values are as follows: mean ± standard deviation (minimum-maximum). P-value was derived from a two-sample t-test comparing variable distributions between females and males. *Abbreviations:* BMI - body mass index; BSA - body surface area; LBW - lean body weight; ICV - intracranial volume.

The 112 subjects (42 / 37.5% females) with manual edits necessary in brain image analysis were about 2 years younger (p=0.0063; non-edited 31±6 years; edited 29±7 years), 5cm taller (p=0.0007; non-edited 170±10cm; edited 175±10cm), with 0.06m^2 higher BSA (p=0.0276) and 3kg higher LBW (p=0.0237). Body weight (p=0.1848), BMI (p=0.4393), and ICV (0.0719; non-edited [1.45±0.22]*10^{6}mm^3; edited [1.51±0.24]*10^{6}mm^3) did not differ. Most variables that differed appear proportional to the higher frequency of manual edits in male brain scans. Seventy-seven of the 112 manually edited scans were acquired with the Siemens MRI scanner (49% of the Siemens scans), 18 of the 112 with the Philips scanner (37%), and 17 of the 112 with the GE scanner (52%).

3.2 Minimal impact of manual segmentation edits on accuracy of brain morphology

BrainGMVol was higher at about 27000mm^3 (estimated error (Eq. 15) +3.8%; p=0.0182) in males and 26400mm^3 (error +2.8%; p=0.0056) in females. CorticalGMVol was higher at about 25600mm^3 (error +4.2%; p=0.0061) in males and 23500mm^3 (error +5.0%; p=0.0028) in females. PrecentralGMVol was higher at about 1400mm^3 (error +5.1%; p=0.0203) in males. Cortical thickness was higher at about 0.04mm (error +1.5%; p=0.0349) in females. Please note that the detected mm thickness error is markedly below the imaging spatial resolution. Otherwise, no differences were observed in brain morphology measurements regarding non-edited and manually edited results (**Supplementary Table 1**). Because all detected errors were ≤5%, we conclude a minimal impact of the utilized manual edits on brain morphology measurements. Contrary, the errors would be much larger without the editing.

$$error = 200*(edited\_mean-non\text{-}edited\_mean)/(edited\_mean+non\text{-}edited\_mean) \quad (15)$$

3.3 Gaussianity of demographic and structural MRI data

Age demonstrated log-Gaussian distribution. Body height demonstrated neither Gaussian (p=0.0089) nor log-Gaussian (p=0.0259) distributions. Body weight, BMI, all CSA measurements, all SC DTI measurements and all brain morphological measurements demonstrated Gaussian distributions. All SC MTR measurements demonstrated neither Gaussian (p<0.0086) nor log-Gaussian (p<0.0009) distributions.

3.4 Body size interacts with the structure of spinal cord white matter

The following CSA measurements were averaged from cervical C3-4 segments (see Methods for details). CSA of SC (CSA-SC) was correlated moderately with body height (r=0.355, **Fig. 1**, **Table 2**), and this correlation strength was higher for the CSA-WM subregion (r=0.437, **Fig. 1**, **Table 2**). CSA-SC and CSA-WM

demonstrated minimal differences between scanner manufacturers (**Fig. 1**). Thus, the same correlation patterns for height were preserved even when manufacturer-specific averages of CSA-SC or CSA-WM were subtracted from corresponding CSA measurements prior to the correlation analysis in order to normalize data across scanners (**Table 2**). The correlation between body height and CSA-SC/CSA-WM remained significant even when the dataset was split into males and females (**Table 2**). Body weight was correlated weakly with CSA-SC (r=0.261) and CSA-WM (r=0.274). In addition, this correlation was not significant when the dataset was split into males and females (**Supplementary Table 2**). CSA-GM was not correlated with body size (**Fig. 1**, **Supplementary Table 2**). The CSA-GM measured on Philips scanners demonstrated a lower mean offset than for data obtained on Siemens and GE scanners (**Fig. 1**; $p<0.0001$). Neither CSA measurement (i.e, SC, WM, GM) was correlated with age (**Fig. 1**, **Supplementary Table 2**). Overall, body height is the demographic variable driving the impact on CSA-WM and explaining the majority of demography-related variability in CSA measurements **(Fig. 2b**, **Supplementary Table 3**). ICV correlated with CSA-WM and CSA-SC less profoundly than body height (**Fig. S1**, **Fig. 1**, **Table 2**).

DTI- and MTR-derived microstructural measurements were averaged from cervical C2-5 levels (see Methods for details). GE-scanner-derived DTI and MTR measurements significantly differed from Siemens and Philips scanners (**Fig. 3**, $p<0.0001$). Therefore, GE scanner microstructural measurements (13.87% of the dataset) were not included in correlation analyses that did not use manufacturer-specific normalized microstructural values (**Table 2**). Body weight was correlated weakly with mean diffusivity (MD) in the WM region (r=-0.200, **Fig. 3**, **Table 2**, **Fig. S2**) and bilateral dorsal columns (DC, r=-0.207, **Fig. S3**). Body weight was not significantly correlated to MD for females (**Table 2**). No investigated DTI measures (i.e., MD, fractional anisotropy - FA or radial diffusivity) were correlated to body size when extracted from the GM region (**Fig. S4**) or bilateral lateral corticospinal tracts (LCST; **Fig. S5**). CSA-WM and SC FA were correlated weakly in DC (r=-0.247) and LCST (r=-0.224). Body weight was correlated weakly to MTR in WM (r=-0.225, **Fig. 3**) DC (r=-0.231, **Fig. S6**) and LCST (r=-0.200, **Fig. S6**), and not correlated to MTR in GM (**Fig. S6**). The correlation between body weight and MTR remained significant, even when the dataset was split into males and females (**Table 2**). When the dataset was normalized for each manufacturer and values from GE scanners were included in the analysis, the correlation values remained almost identical (**Table 2**). This finding signifies that the observed effect remained identical but had slightly higher power due to the larger sample size (added 37 samples; +13.87%). The correlation analysis revealed no aging effects in DTI ($-0.004 \geq r \geq -0.099$) or MTR ($-0.047 \geq r \geq -0.094$) measures (**Fig. S2-6**) in our sample. However, the exploratory principal component analysis showed small effects in mutual covariance (**Fig. 7d**). Linear regression analysis showed that body weight explained the majority of the demography-related variance in our young adult sample DTI and MTR measurements (**Supplementary Table 3**).

3.5 Body height, ICV, and age interact with brain morphology

Body height was correlated moderately with several cerebral volumes ($r=0.54\pm0.06$; $0.434 \leq r \leq 0.622$), i.e., volumes of the brain, brain GM, cortical GM, cortical WM, subcortical GM, thalamus, cerebellum, brainstem, precentral GM and postcentral GM (**Fig. 4**, **Fig. 5a**). The vast majority of correlations with body height remained significant even after the dataset was split to males and females, except for the volumes of cortical WM, subcortical GM, precentral GM and postcentral GM in females (**Table 2**). The body height interacted most profoundly with the cortical GM volume (**Fig. 2b**).

Body weight demonstrated weaker correlations in all the cortical regions that correlated moderately with body height ($r=0.37\pm0.07$, **Fig. 4**, **Fig. 5a**, **Supplementary Table 2**). The only significant correlation that survived the dataset split to males and females was brainstem volume in males (**Table 2**).

Body height or body weight were not correlated with total cortical, precentral gyrus, and postcentral gyrus thicknesses (**Fig. 5a**).

ICV correlated with brain morphology more profoundly than body height (**Table 2, Fig. S1, Fig. 4**, **Fig. 5a**). Yet, regarding the low-to-moderate correlation coefficients between ICV and body size (**Table 2**), we assume that ICV and body size do not share entropy entirely. Thus, all effects in brain morphology cannot be explained by ICV only.

As expected, a weak manifestation of age-related cortical GM atrophy was observed in volume (r=-0.213) and thickness (r=-0.274) measures (**Fig. 4**, **Fig. 5a**). The aging GM atrophy effects remained significant after the dataset split to males and females (**Table 2**).

Most importantly, the magnitude of linear dependence between brain morphology and body height (or ICV) was about 2- to 3-fold compared to the effects of age (**Table 2**, **Fig. 4**, **Fig. 5a**). Moreover, the young adult dataset showed that body height and ICV explain more, pathology unrelated, variance in brain volumetry than age and sex (**Supplementary Table 3**). Contrary, cortical thickness variance was associated predominantly with age (**Supplementary Table 3**).

3.6 Body size or concurrent body mass measurements?

BMI was highly linearly dependent on body weight (r_{BMI}=0.801). BSA and LBW were highly linearly dependent on body height (r_{BSA}=0.864; r_{LBW}=0.867) and weight (r_{BSA}=0.964; r_{LBW}=0.933) favoring effects of the weight against the height in the final measurement. Therefore, neither BMI, BSA and LBW demonstrated higher linear dependence effects with CNS morphology than were observed for the body height (**Fig. S7-9** vs **Fig. 1**, **Fig. 4**, **Fig. 5a**). BMI, BSA and LBW do not seem to increase correlation magnitude with SC MTR when compared to body weight (**Fig. S10** vs **Fig. 3**). However, LBW may increase the correlation magnitude with SC DTI (**Fig. S10** vs **Fig. 3**).

3.7 Body size and ICV improves prediction of CNS structure

Linear regression of age itself explained only 2±2% of investigated CNS morphology variance (**Supplementary Table 3**). Utilizing body height (R^2=27±8%), sex (R^2=24±10%) or ICV (R^2=36±16%) separately explained a significant portion of variance in CNS morphology (**Supplementary Table 3**). However, the amount of explained variance in CNS morphology was maximized when a linear mixture of all four variables were modeled together (R^2=46±17%; **Supplementary Table 3**). Stepwise linear regression identified age, body height and ICV as significant variables determining investigated CNS morphological measurements (R^2=45±17%; **Table 3**). Sex was an additional significant variable in predictions of cerebellar, brainstem, and subcortical GM volumes (**Table 3**). Pearson correlation coefficient between measured and predicted CNS morphology increased from r=0.58±0.15 to r=0.66±0.13 when compared to ICV correlations (**Table 3**). *Utilizing male dataset only:* The identified set of significant variables predicting CNS morphology remained very similar. Additionally, body weight was identified as an additional variable in some measurements. Explained CNS morphology variance was R^2=38±18% and the Pearson correlation coefficient increased from r=0.52±0.16 to r=0.60±0.16 when compared to ICV correlations (**Supplementary Table 4**). *Utilizing female dataset only:* The identified set of significant variables predicting CNS morphology remained very similar to male and both sex models. However, the explained variance was only 20±9% and the correlation coefficient increase was from r=0.31±0.15 to r=0.43±0.11, suggesting unidentified biological factor/s further determining the CNS morphology in young adult females (**Supplementary Table 5**).

Body weight explained ≈5% variance in SC microstructure measured with DTI or MTR (**Supplementary Tables 3-5**; **Table 3**). When the dataset was split into males or females only, body weight was not identified as a significant variable determining DTI (**Supplementary Tables 4** and **5**). Age explained ≈8% variance in cortical thickness measurements (**Supplementary Tables 3-5**; **Table 3**).

CNS structural measurements and root mean square errors (RMSE) of all model predictions are listed in **Table 3** and **Supplementary Tables 4** and **5**. In all cases, the RMSE was lower than standard deviation of the structural measurement (**Table 3**, **Supplementary Tables 4** and **5**).

3.8 Cross-sectional area of spinal cord white matter interacts with brain morphology

CSA-SC (r=0.38±0.09; 0.240≤r≤0.575) and CSA-WM (r=0.48±0.07; 0.389≤r≤0.640) were correlated moderately with the investigated brain volumes, i.e., volumes of the brain, brain GM, cortical GM, cortical WM, subcortical GM, thalamus, cerebellum, brainstem, precentral GM, and postcentral GM (**Fig. 5b**, **Fig. 6**, **Table 2**). Compared to CSA-SC, correlation strengths were higher for CSA-WM (**Fig. 5b**, **Fig. 6**, **Table 2**). CSA-GM was correlated weakly with the volume of the brain, cortical WM, subcortical GM, and brainstem, but the strength of these correlations was half weaker than those observed for CSA-SC and CSA-WM (**Fig. 6**, **Table 2**). All CSA-WM and most of the other observed correlations remained significant after the dataset split to females and males (**Table 2**) or when SC data were normalized (zero mean) for each manufacturer prior to correlation analysis (**Table 2**). CSA-WM was the primary marker defining the correlations with the brain volumes. There was a descending gradient of the CSA-WM correlation from the brainstem to subcortical GM and then cortical WM to the cortical GM (**Fig. 2c**). All these correlations were higher than the correlation with the volume of the cerebellum (**Fig. 2c**). Yet, even the correlation between CSA-WM and cerebellum volume was significant **(Fig. 2c**, **Fig. 6**).

CSA-SC (r=0.211) and CSA-WM (r=0.252) were correlated weakly with the thickness of the precentral gyrus (**Fig. 5b**). The correlations remained significant after the dataset split to females and males (**Table 2**). However, the correlations disappeared when SC data were normalized before correlation analysis (**Table 2**). CSA-GM was not correlated with any utilized cortical thickness measurement (**Fig. 5b**).

3.9 Brain morphology and spinal cord microstructure are not related

No correlations were detected between SC WM/GM microstructure and cerebral volumes (i.e., total brain, brain GM, cortical GM, cortical WM, subcortical GM, thalamus, cerebellum, brainstem, precentral GM and postcentral GM) or cortical thickness (**Fig. S11-12**), and between thickness measurements and DTI/MTR measurements, even if the SC ROIs were limited to the bilateral LCST or DC (**Fig. S13-15**).

3.10 ICV normalization of brain volumes emphasizes ICV information in the measurements

ICV normalization of volumes of different brain regions reduced correlation levels with body height and weight (**Fig. S16** vs **Fig. 4**, **Fig. 5a**). But the normalization also reduced variance/entropy about the brain structure itself in the measurement because the normalized brain volumes (x_{norm}) correlated more strongly with ICV^{-1} (r=0.72±0.07; min 0.58; max 0.83; **Fig. S16**) than with original volumes (x; r=0.12±0.19; min -0.14; max 0.42). Moreover, the ICV normalization emphasized scanner-effects in the brain volume measurements. ICV normalization of brain volumes generated a distinct cluster of GE measurements (**Fig. S16**) that was not observed in non-normalized brain volume measurements (**Fig. 4**, **Fig. 5a**). Both brain volumes and ICV were measured with FreeSurfer v7.2. In 14 (8.9%) Siemens and 4 (8.2%) Philips T1w scans, ICV was estimated lower than the unnormalized brain volume. Therefore, the Freesurfer software provided unphysiological normalized brain volumes >100% in such scans (**Fig. S16**). The utilized brain and intracranial volume variables are called BrainSegVol and eITV in the FreeSurfer software. Further detail origin of such software error is unknown to us at the moment. Image visual inspection did not identify any obvious pitfall in these 18 cases.

3.11 Scanner-related effects on SC structural measurements

CSA-SC and CSA-WM offsets differed minimally between manufacturers (**Fig. 1**, **Fig. 5b**, **Fig. 6**). CSA-GM measurements on Philips scanners were significantly lower than CSA-GM measurements from Siemens and GE scanners (**Fig. 1**, **Fig. 5b**, **Fig. 6**, p<0.0001). Additional discussion about this specific CSA-GM issue can be found in (Cohen-Adad et al., 2021b). Data normalization before correlation analysis mainly decreased the correlation strengths in all CSA measures (without normalization: r=0.348±0.127; with normalization r=0.313±0.128; **Table 2**; paired t-test p<0.0001). This finding underlines the importance of adjusting for scanner-related variability in CSA measurements to minimize risks of false positive results due to scanner-related data trends.

All microstructural measurements obtained with GE scanners showed significant offsets compared to those from Siemens and Philips scanners (**Fig. 3**, **Fig. S2-6**, **Fig. S10-15**, $p<0.0001$). The differences had a direct impact on correlation analyses. Therefore, we performed correlation analyses of original values without GE values and correlation analyses of normalized values utilizing all scanners' data. Correlation analyses were stable and comparable in the magnitude of correlation coefficients for MTR (**Table 2**) and MD (**Table 2**). The normalized correlation analysis provided higher statistical power due to the larger sample size. Additionally, if we utilized GE data (**Fig. 3**) in the correlation analysis without normalization, the resulting correlation coefficients for MD-SC-WM and MTR-SC-WM in **Table 2** would be substantially lower.

3.12 Minimal impact of degenerative cervical spinal cord compression on correlation analysis

We excluded one participant with severe degenerative cervical SC compression that introduced outliers in SC structural measurements. However, the *spine-generic* database identifies an additional 61 subjects with mild degenerative compression and 2 subjects with severe degenerative compression and radiological myelopathy (Valošek et al., 2024). Analysis power decreased, but minimal nuances were detected in correlation coefficients when tested separately on subjects without or with degenerative cervical SC compression (see **Supplementary Slides**). Thus, we conclude that SC compression had a minimal impact on the current study outcomes.

3.13 Principal component analysis (PCA) reveals body-SC-brain structural links

We subtracted manufacturer-specific average values from all SC structural measurements prior to the exploratory analysis via PCA. PCA did not include DTI and MTR measurements from bilateral LCST and DC, as the WM region provided analogic observations. Cerebral volumes, CSA-WM, body height and ICV formed the first principal component (PC1), characterizing 44.00% of data variance (**Fig. 7a**). CSA-SC and body weight were close, yet separated from the PC1 cluster (**Fig. 7a**). This finding supports the previously observed body height and CSA-WM dominance in the observed effects (**Fig. 1**, **Fig. 2**, **Fig. 4**, **Fig. 5**, **Fig. 6**, **Table 2**, **Table 3**). Cortical thickness, MD-SC-WM, and age (negative effect) formed the second principal component (PC2), characterizing 12.06% of data variance (**Fig. 7a**) and presenting predominantly negative aging effects in the thickness measures. The PC1-PC3 projection showed that the PC3 characterizes about 8.65% of data variance, predominantly explained by CSA-GM, MD-SC-WM, and FA-SC-GM (negative effect), i.e., a link between SC GM morphology and SC microstructure (**Fig. 7b**). The PC2-PC3 projection verified that the cortical thickness variability predominantly forms PC2. In contrast, PC3 is predominantly formed by SC DTI and CSA-GM (**Fig. S17a**). PC4 explained 5.51% of unique SC DTI microstructural data variance, which is not present in other investigated modalities and investigated demographic measures (**Fig. 7c**). PC5 showed positive effects of body weight and age on MD-SC-WM, and negative effects of body weight and age on MTR-SC-WM, FA-SC-GM, and CSA-GM. These effects explained about 4.56% of data variance (**Fig. 3**, **Fig. 7d**). Simultaneously, the PC projections suggest that the impact of body weight on MTR- and DTI-derived microstructure metrics might be ≈5% (**Fig. 3**, **Fig. 7**). That follows the result of explained variance in the regression analyses (**Supplementary Table 3**, **Table 3**). However, the positive effects of body weight on MD-SC-WM contradicts our observation of weak negative correlation between body weight and SC MD (**Fig. 3**). PC3 and PC5 showed clear evidence that CSA-GM morphology and SC microstructure are linked, yet unrelated to cerebral and SC WM morphology (**Fig. 7b,d**, **Fig. S17a**). In summary, PCA analysis explained 75% of data variance, and roughly 25% is unexplained (**Fig. S17b**).

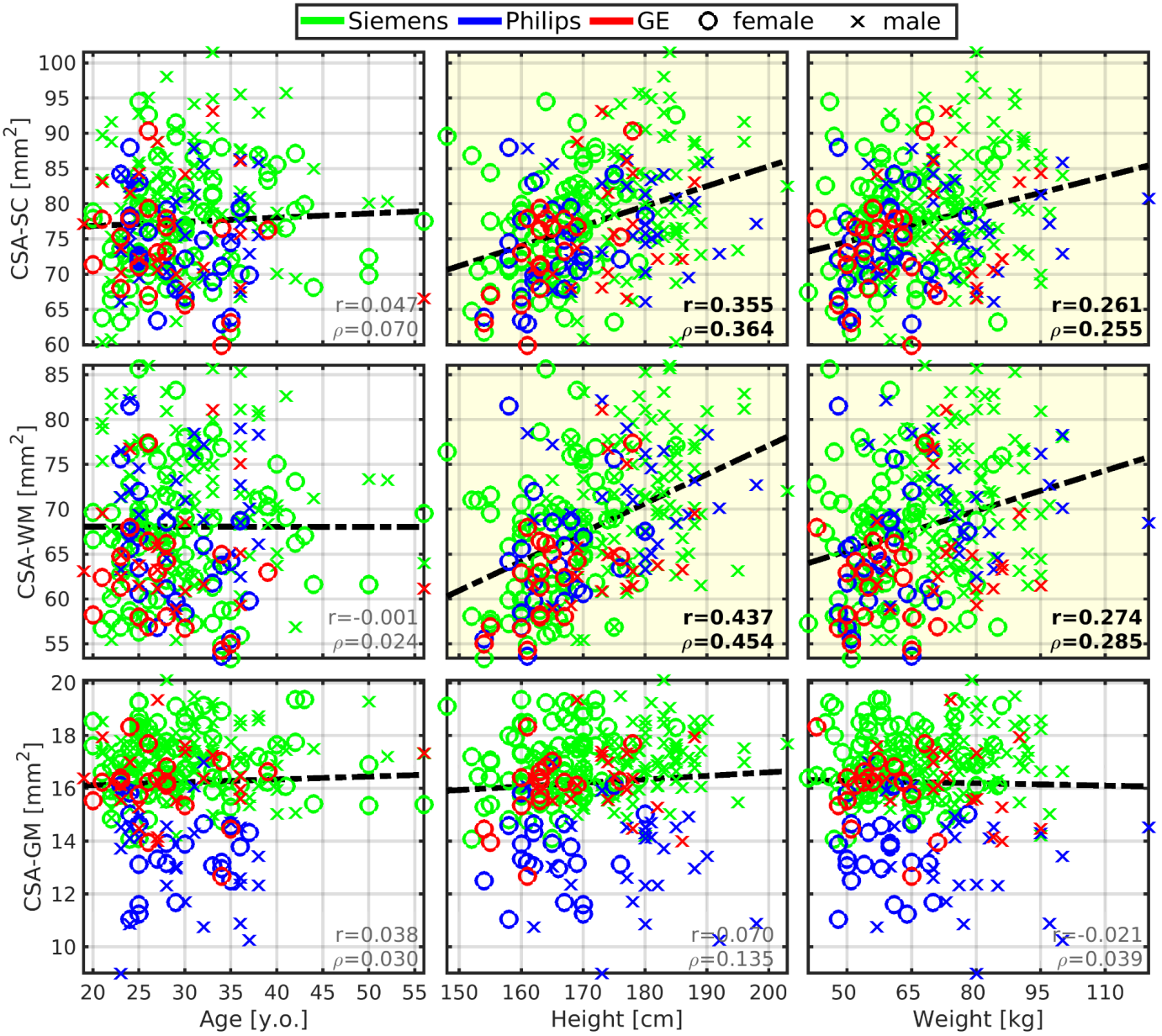

Figure 1: Cross-sectional area of spinal cord white matter correlates with body height and weight.
Abbreviations: CSA - cross-sectional area; SC - spinal cord; WM - white matter; GM - gray matter; r - Pearson correlation coefficient; ρ - Spearman correlation coefficient. All spinal cord measurements were averaged from cervical C3-4 levels. Regression lines (i.e., the dashed black lines) were estimated from all available data points. Plots with statistically significant correlation (p_{FWE}<0.05) are highlighted with yellow background, and corresponding r and ρ values are highlighted with black bold font.

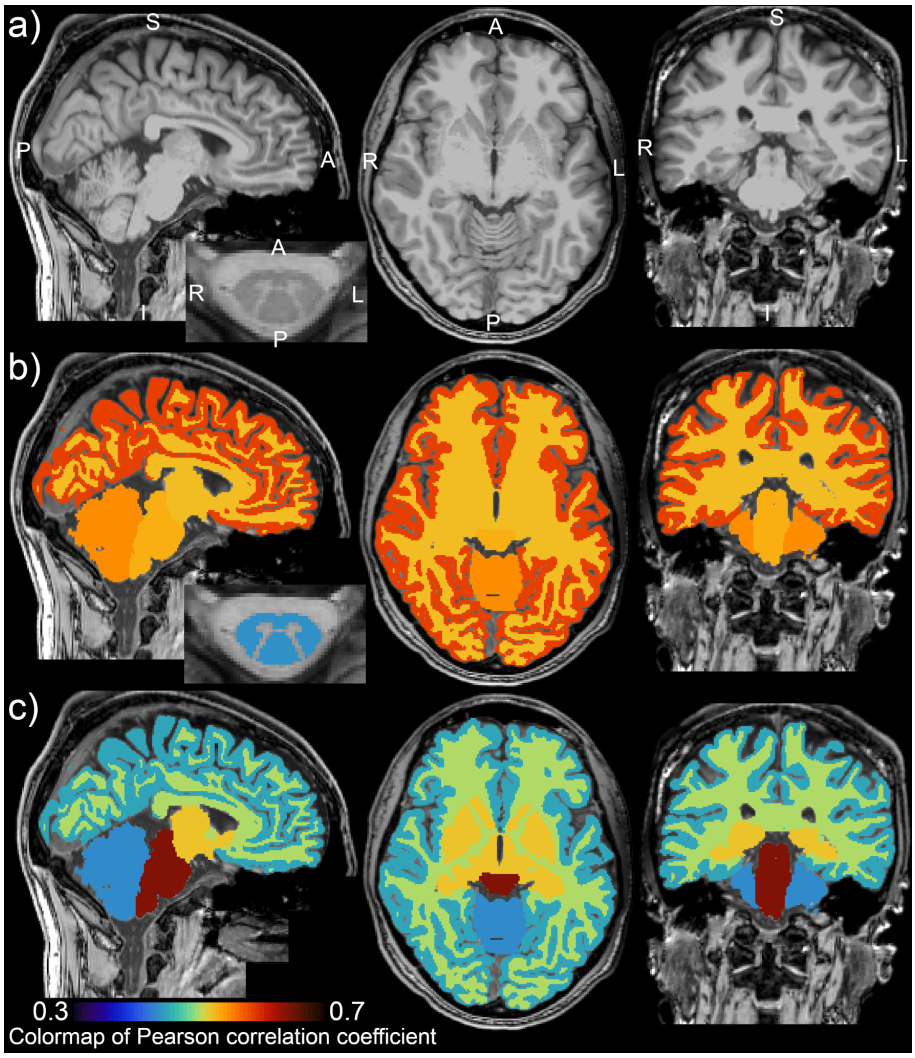

Figure 2: Pearson correlation coefficient maps showing interactions between body height and morphology of the central nervous system.

Panel a) Representative image of brain and spinal cord (SC) anatomy. The brain scan shows cortical gray matter (GM), cerebral white matter (WM), subcortical GM structures, brainstem and cerebellum. The axial SC scan shows the WM and GM anatomy at the C3/C4 level. Image orientation is described in **panel a)**: A - anterior, P - posterior, S - superior, I - Inferior, L - left and R - right. **Panel b)** Pearson correlation coefficient between body height and (i) cortical GM volume; (ii) cerebral WM volume; (iii) subcortical GM structure volume; (iv) brainstem volume; (v) cerebellar volume; and (vi) cross-sectional area (CSA) of cervical SC WM at C3/C4 level. The colormap for the correlation values is shown in the left bottom corner of the figure. All correlations are significant ($p_{FWE}<0.05$). Regarding the investigated list of structures, body height demonstrated the strongest correlation with the cortical GM volume. **Panel c)** Pearson correlation coefficient between the CSA of cervical WM at C3/C4 level and (i) cortical GM volume; (ii) cerebral WM volume; (iii) subcortical GM structure volume; (iv) brainstem volume; and (v) cerebellar volume. The colormap for the correlation values is shown in the left bottom corner of the figure. All correlations are significant ($p_{FWE}<0.05$). The correlation map shows a descending gradient from the brainstem through subcortical GM structures and cerebral WM to cortical GM. The gradient may be driven by the increasing distance to the cervical SC level and decreasing relative volume of common tract pathways. The cerebellum shows the lowest, yet significant, correlation level. This finding may be explained by the fact that the cerebrum is more strongly and directly interconnected to the peripheral nervous system via SC than the cerebellum, with spinocerebellar tracts as the primary direct connections (Chandar & Freeman, 2014; Purves et al., 2001).

Table 2: Pearson correlation coefficients between body size, age, spinal cord structure, brain structure, and intracranial volume, and post-hoc sex-effects in the correlation analysis.

Abbreviations: CSA - cross-sectional area; SC - spinal cord; WM - white matter; GM - gray matter; Vol - volume. The correlation analysis on non-normalized data identified a list of variable pairs with a correlation coefficient of $p_{FWE}<0.05$. The final list here only selects the variable pairs with a significant post-hoc Pearson correlation coefficient (uncorrected $p<0.05$ in at least one sex-specific sub-dataset (i.e., female and/or male). Insignificant correlation coefficients, that did not meet the post-hoc condition uncorrected $p<0.05$, are written with gray font. Positive correlation coefficients ($p<0.05$) are visualized as a yellow-orange-pink-red color shade of the table background. Negative correlation coefficients ($p<0.05$) are visualized as a light blue-blue color shade of the table background. CSA was measured as averages between C3-C4 segments. DTI and MTR were calculated as averages between C2-C5 segments. The column denoted *"Original values"* reports correlation coefficients for raw measurements with no normalization procedure prior to the correlation analysis. The column denoted *"Manufacturer-specific normalized SC measures"* reports correlation coefficients for SC structural measurements, which were normalized to zero mean for each scanner manufacturer before correlation analysis. Empty cells in the right half of the table represent combinations where no updated correlation coefficients were measured, because the utilized normalization of SC structural measurements had no effect on these correlation coefficients. Brain structural measurements were not considered necessary to normalize as we did not observe strong scanner-related effects in brain macrostructural measurements.

Grouping Variable	Correlated variable	Original values (no data normalization)			Manufacturer-specific normalized SC measures		
		All	Female	Male	All	Female	Male
INTRACRANIAL VOLUME	Height	0.463	0.045	0.226			
	Weight	0.357	-0.117	0.124			
	BrainVol	0.773	0.522	0.750			
	BrainGMVol	0.703	0.412	0.663			
	CorticalWMVol	0.723	0.507	0.666			
	CorticalGMVol	0.684	0.420	0.644			
	SubCortGMVol	0.673	0.389	0.604			
	ThalamusVol	0.558	0.372	0.435			
	CerebellumVol	0.556	0.225	0.470			
	PrecentralGMVol	0.524	0.230	0.461			
	PostcentralGMVol	0.526	0.290	0.504			
	BrainStemVol	0.500	0.145	0.396			
	CSA-WM	0.370	0.140	0.304	0.413	0.210	0.342
	CSA-SC	0.300	0.108	0.273	0.312	0.132	0.279
HEIGHT	BrainGMVol	0.622	0.321	0.446			
	BrainVol	0.611	0.274	0.409			
	CorticalGMVol	0.583	0.252	0.449			
	CerebellumVol	0.546	0.411	0.219			
	BrainStemVol	0.530	0.310	0.259			
	CorticalWMVol	0.522	0.157	0.313			
	SubCortGMVol	0.521	0.107	0.288			
	PrecentralGMVol	0.495	0.092	0.418			
	CSA-WM	0.437	0.295	0.303	0.422	0.285	0.268
	PostcentralGMVol	0.434	0.121	0.369			
	CSA-SC	0.355	0.323	0.230	0.344	0.319	0.205
WEIGHT	BrainStemVol	0.431	0.119	0.191			
	MD-SC-WM	-0.200	-0.022	-0.191	-0.252	-0.108	-0.206
	MTR-SC-WM	-0.225	-0.374	-0.221	-0.221	-0.331	-0.217
AGE	CorticalGMVol	-0.213	-0.357	-0.257			
	PrecentralGMVol	-0.205	-0.326	-0.232			
	Cortical Thickness	-0.274	-0.278	-0.277			
CSA-WM	BrainStemVol	0.350	0.624	0.533	0.585	0.580	0.454
	BrainVol	0.519	0.392	0.445	0.503	0.379	0.413
	SubCortGMVol	0.506	0.257	0.508	0.483	0.248	0.459
	CorticalWMVol	0.498	0.315	0.456	0.496	0.339	0.432
	BrainGMVol	0.479	0.341	0.397	0.443	0.286	0.351
	CorticalGMVol	0.447	0.283	0.383	0.411	0.227	0.340
	CerebellumVol	0.430	0.501	0.170	0.438	0.508	0.177
	ThalamusVol	0.421	0.244	0.373	0.441	0.279	0.384
	PrecentralGMVol	0.420	0.235	0.382	0.370	0.178	0.317
	PostcentralGMVol	0.389	0.243	0.356	0.345	0.181	0.311
	PrecentralG Thickness	0.252	0.249	0.209	0.146	0.142	0.087
CSA-SC	BrainStemVol	0.572	0.622	0.485	0.517	0.573	0.403
	BrainVol	0.417	0.337	0.361	0.391	0.311	0.321
	SubCortGMVol	0.415	0.207	0.441	0.387	0.198	0.385
	CorticalWMVol	0.430	0.291	0.414	0.409	0.280	0.377
	BrainGMVol	0.357	0.265	0.283	0.324	0.225	0.239
	CorticalGMVol	0.319	0.195	0.259	0.291	0.159	0.223
	CerebellumVol	0.355	0.508	0.104	0.341	0.493	0.082
	ThalamusVol	0.329	0.176	0.308	0.333	0.201	0.296
	PrecentralGMVol	0.307	0.159	0.273	0.275	0.132	0.228
	PostcentralGMVol	0.240	0.146	0.184	0.218	0.120	0.160
	PrecentralG Thickness	0.211	0.180	0.201	0.144	0.125	0.117
CSA-GM	BrainStemVol	0.390	0.444	0.478	0.335	0.440	0.376
	BrainVol	0.221	0.250	0.296	0.186	0.219	0.255
	SubCortGMVol	0.216	0.093	0.389	0.197	0.119	0.344
	CorticalWMVol	0.267	0.275	0.352	0.218	0.215	0.302

Fitted model: $y \propto y_0 + \sum b_i * x_i$	R^2	R^2_{ICV}	R^2_{Height}	r	r_{ICV}	RMSE	y (mean ± STD)
BrainGMVol ∝ 42252 -1943*Age +2593*Height +0.164*ICV	63.6%	49.4%	38.7%	0.797	0.703	42399mm^3	673668±70031mm^3
BrainVol ∝ -35072 +4215*Height +0.354*ICV	68.0%	59.8%	37.4%	0.824	0.773	73122mm^3	1213993±128729mm^3
CorticalGMVol ∝ 35408 -1778*Age +1834*Height +0.13*ICV	59.7%	46.7%	34.0%	0.772	0.684	35417mm^3	490600±55570mm^3
CerebellumVol ∝ 48271 -348*Age +446*Height +0.025*ICV +6953*Sex	44.4%	30.9%	29.8%	0.666	0.556	13028mm^3	151930±17344mm^3
BrainStemVol ∝ 5814 +71.6*Height +0.003*ICV +1069*Sex	38.5%	25.0%	28.1%	0.620	0.500	2049mm^3	22613±2597mm^3
CorticalWMVol ∝ -3594 +1465*Height +0.165*ICV	56.9%	52.2%	27.2%	0.754	0.723	40055mm^3	491753±60605mm^3
SubCortGMVol ∝ 29015 +91*Height +0.012*ICV +2474*Sex	53.0%	45.3%	27.2%	0.728	0.673	3989mm^3	62987±5804mm^3
PrecentralGMVol ∝ 1702 -111*Age +114*Height +0.0061*ICV	39.1%	27.5%	24.5%	0.625	0.524	2865mm^3	27103±3641mm^3
PostcentralGMVol ∝ 1217 -50.5*Age +67.3*Height +0.0054*ICV	33.8%	27.6%	18.8%	0.582	0.526	2344mm^3	19197±2858mm^3
CSA-WM ∝ 14.23 +0.242*Height +8e-06*ICV	25.6%	17.1%	17.8%	0.506	0.370	6.2mm^2	68.1±7.4mm^2
CSA-SC ∝ 29.88 +0.224*Height +6e-06*ICV	15.5%	9.7%	11.8%	0.394	0.300	7.4mm^2	77.4±8.0mm^2
MD-SC-WM ∝ 1.030 -0.0012*Weight	4.3%	0.3%	2.2%	0.252	-0.015	0.08*10^{-9}m^2/s	(0.95±0.13)*10^{-9}m^2/s
MTR-SC-WM ∝ 50.3 -0.037*Weight	5.1%	1.5%	0.8%	0.221	-0.116	2.1%	47.5±3.7%
Cortical Thickness ∝ 2.57 -0.0037*Age	7.6%	0.2%	0.8%	0.274	0.042	0.08mm	2.46±0.09mm

Table 3: Stepwise linear regression fitted models predicting CNS structural measure (y).

Abbreviations: ICV - intracranial volume; CSA - cross-sectional area; SC - spinal cord; WM - white matter; GM - gray matter; Vol - volume; SubCort - subcortical; ***y*** - CNS measured structure; y_0 - model constant member (intersect); b_i - regression coefficient of *i-th* variable *x*; *x* - regressed significant variable (e.g. Height, ICV, etc.); R^2 - coefficient of determination for the stepwise fitted model; R^2_{ICV} - coefficient of determination for fitted linear regression model utilizing sex, age and ICV variables; R^2_{Height} - coefficient of determination for fitted linear regression model utilizing sex, age and body height variables; r - Pearson correlation coefficient between measured ***y*** and stepwise model predicted ***y***; r_{ICV} - Pearson correlation coefficient between measured ***y*** and ICV; RMSE - root mean square error between measured ***y*** and stepwise model predicted ***y***; STD - standard deviation.

All variables listed in the fitted models met the statistical threshold condition $p<0.05$. In all cases, the stepwise linear regression fitted model explained more data variance than concurrent linear mixture model utilizing sex, age and ICV (R^2_{ICV}); or sex, age and body height (R^2_{Height}), respectively. Coefficients of determination for other investigated mixture models are listed in the **Supplementary Table 3**. Pearson correlation coefficient also increased for the stepwise fitted model when compared to correlation levels with ICV (r_{ICV}) or body height (**Table 2**) separately.

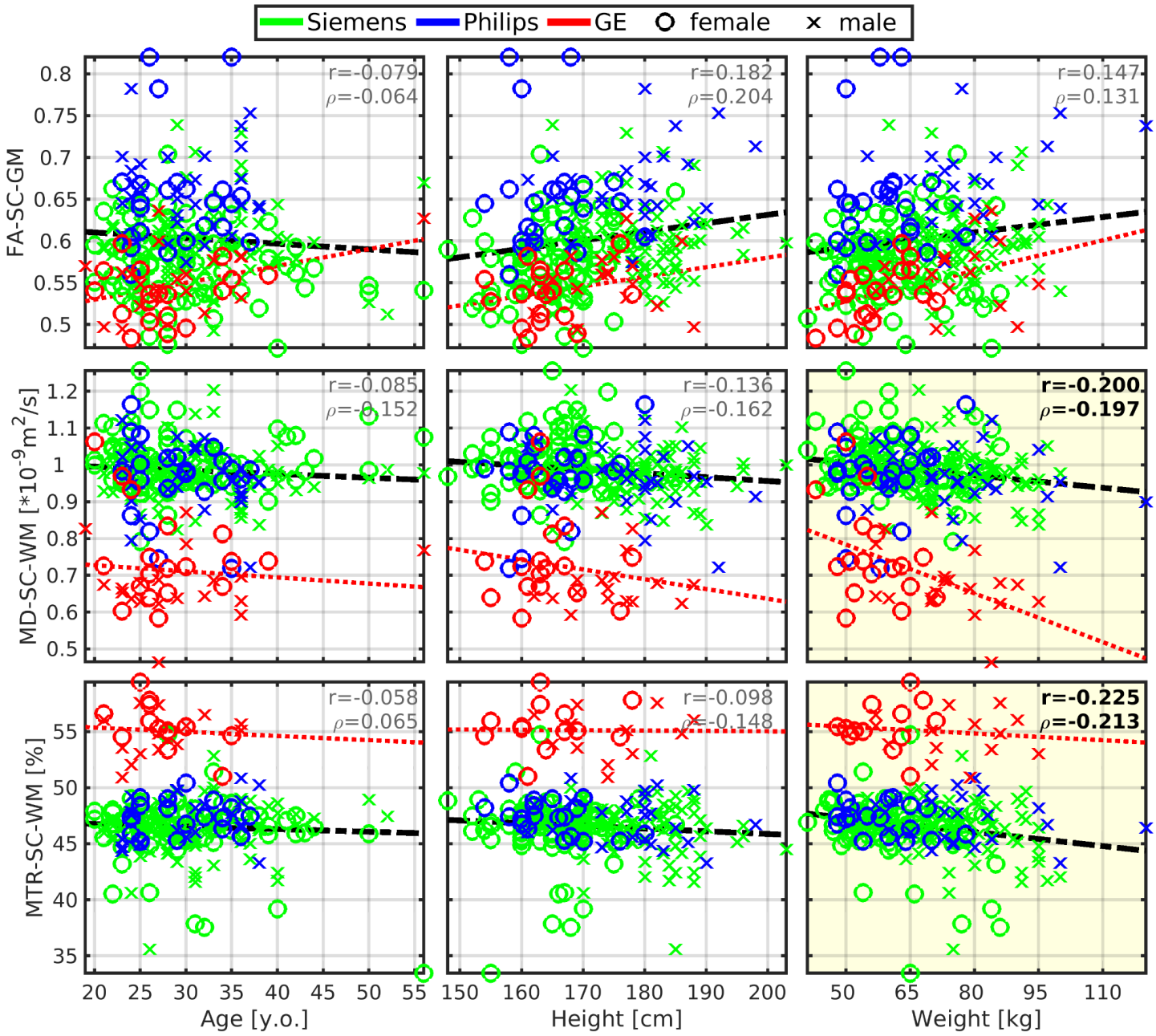

Figure 3: Mean diffusivity and magnetization transfer ratio in spinal cord white matter correlates with body weight.

Abbreviations: GM - gray matter; WM - white matter; SC - spinal cord; FA - fractional anisotropy; MD - mean diffusivity; MTR - magnetization transfer ratio; r - Pearson correlation coefficient; ρ - Spearman correlation coefficient. All spinal cord measurements were averaged from cervical C2-5 levels. Black dashed regression lines were estimated from the Siemens and Philips scanners' data points. Red dotted regression lines were estimated from the GE scanner's data points. Plots with statistically significant correlation ($p_{FWE}<0.05$) are highlighted with yellow background, and corresponding r and ρ values are highlighted with black bold font.

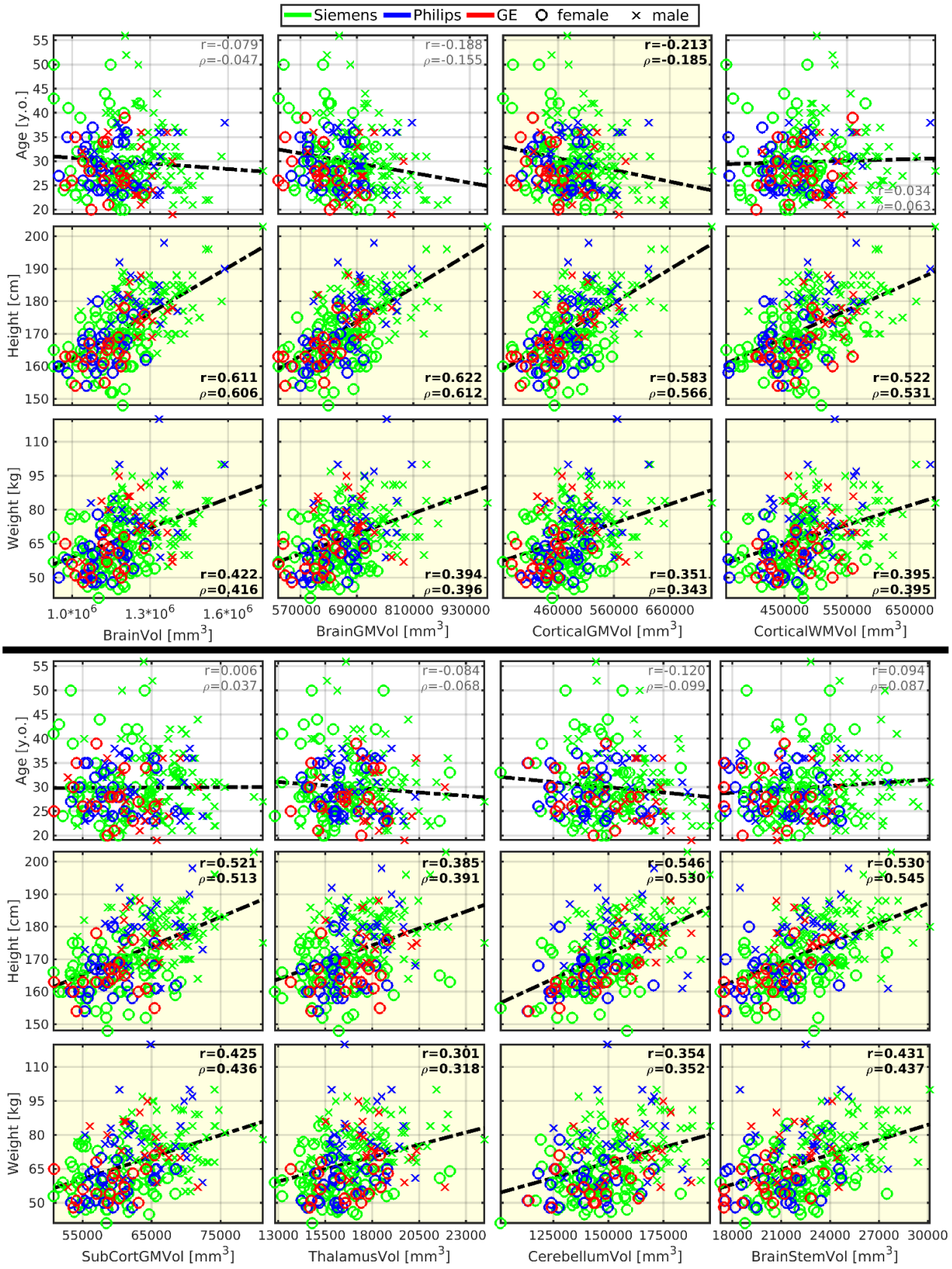

Figure 4: Brain morphology strongly correlates with body size but weakly with age.

Abbreviations: GM - gray matter; WM - white matter; Vol - volume; SubCort - subcortical; r - Pearson correlation coefficient; ρ - Spearman correlation coefficient. Regression lines (i.e., the dashed black lines) were estimated from all available data points. Plots with statistically significant correlation (p_{FWE}<0.05) are highlighted with yellow background, and corresponding r and ρ values are highlighted with black bold font.

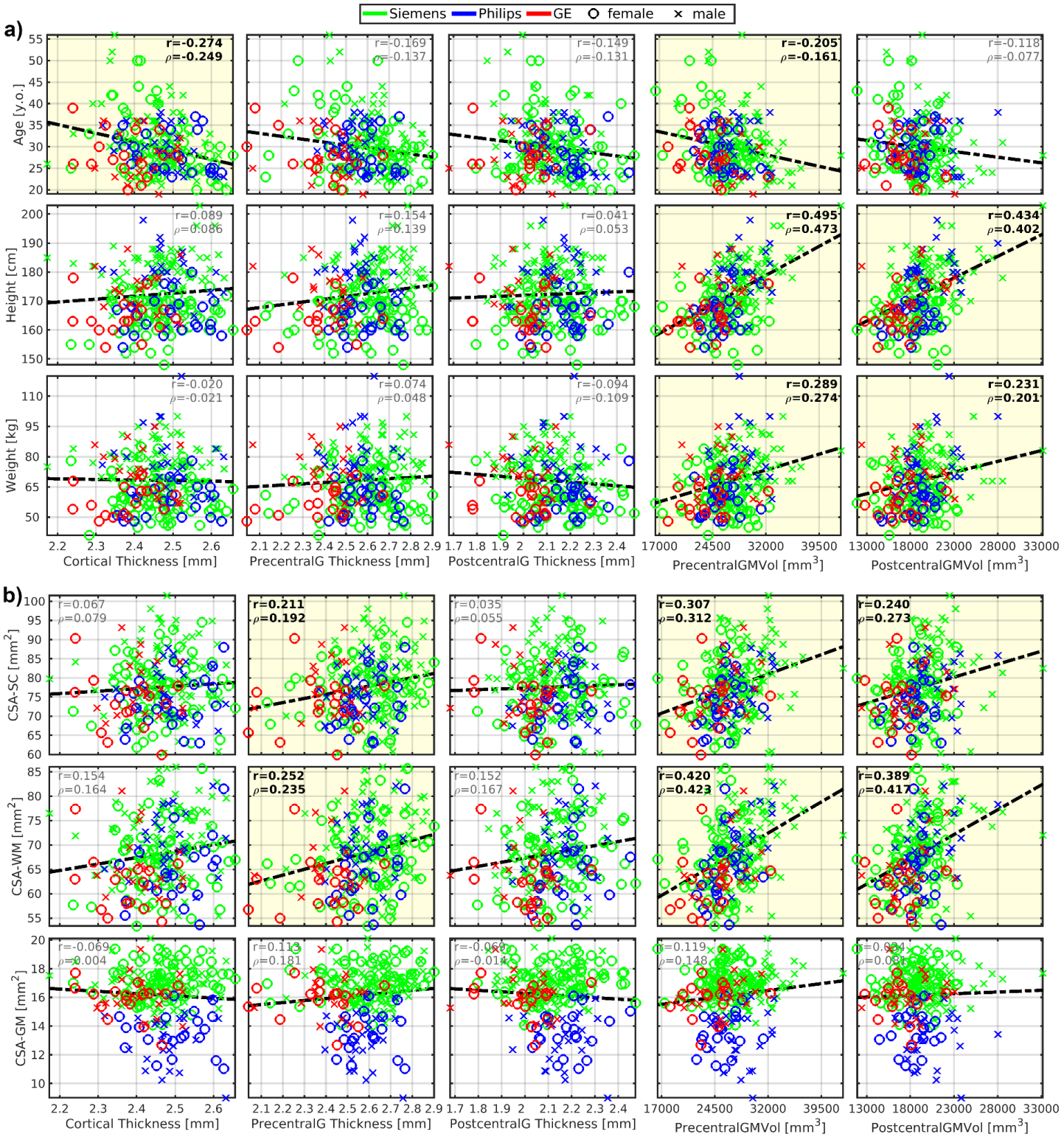

Figure 5: Cortical morphology correlates with body size, age, and cross-sectional area of the spinal cord white matter.

Abbreviations: CSA - cross-sectional area; SC - spinal cord; WM - white matter; GM - gray matter; PrecentralG - precentral gyrus; PostcentralG - postcentral gyrus; Vol - volume; r - Pearson correlation coefficient; ρ - Spearman correlation coefficient. Regression lines (i.e., the dashed black lines) were estimated from all available data points. Plots with statistically significant correlation (p_{FWE}<0.05) are highlighted with yellow background, and corresponding r and ρ values are highlighted with black bold font. **a)** Graphs demonstrate correlations with body size and age. **b)** Graphs demonstrate correlation with CSA measured in the SC region as averages from cervical C3-4 levels.

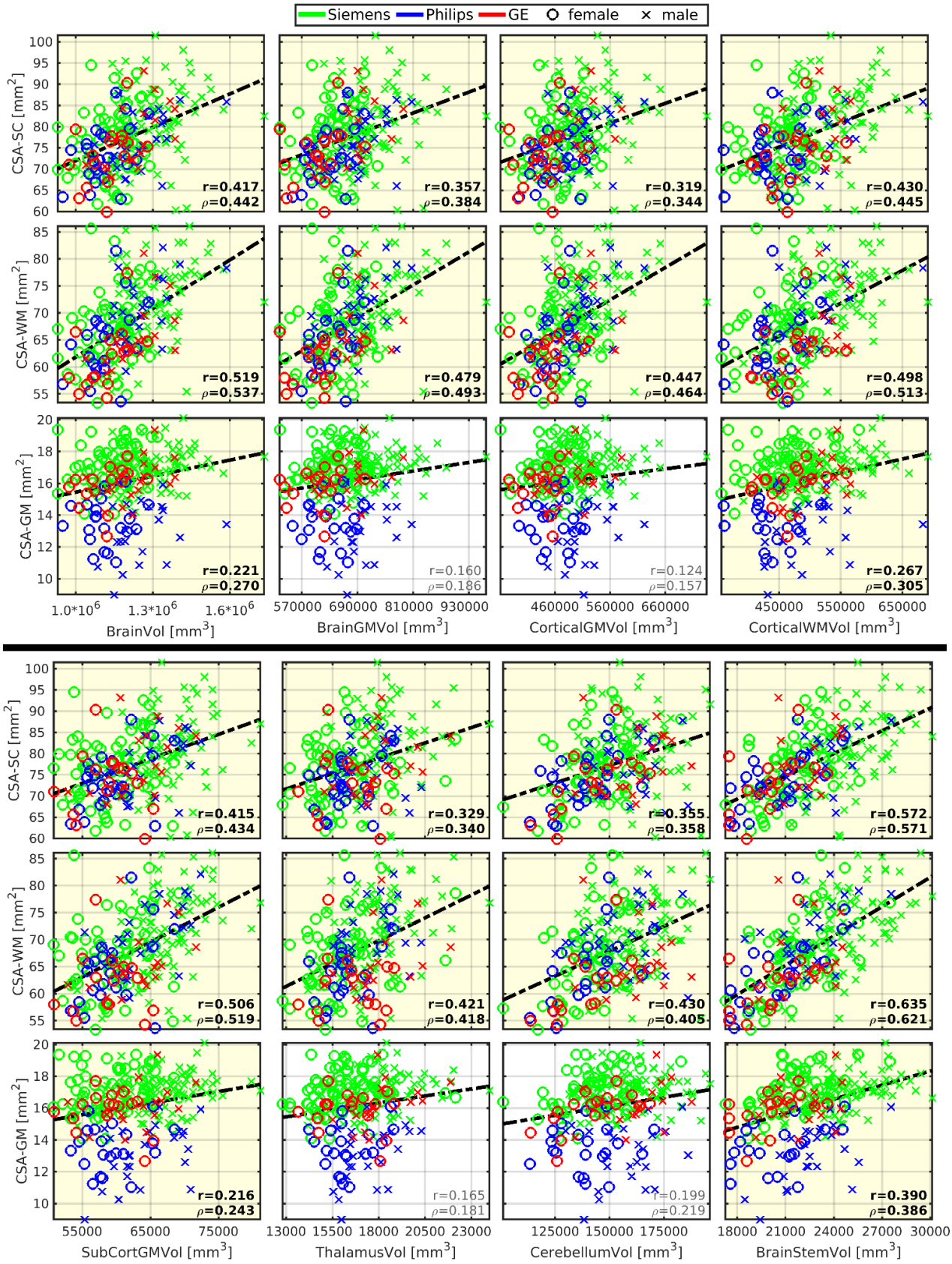

Figure 6: Brain morphology correlates with spinal cord morphology.

Abbreviations: CSA - cross-sectional area; SC - spinal cord; WM - white matter; GM - gray matter; Vol - volume; SubCort - subcortical; r - Pearson correlation coefficient; ρ - Spearman correlation coefficient. All SC measurements were averaged from cervical C3-4 levels. Regression lines (i.e., the dashed black lines) were estimated from all available data points. Plots with statistically significant correlation (p_{FWE}<0.05) are highlighted with yellow background, and corresponding r and ρ values are highlighted with black bold font.

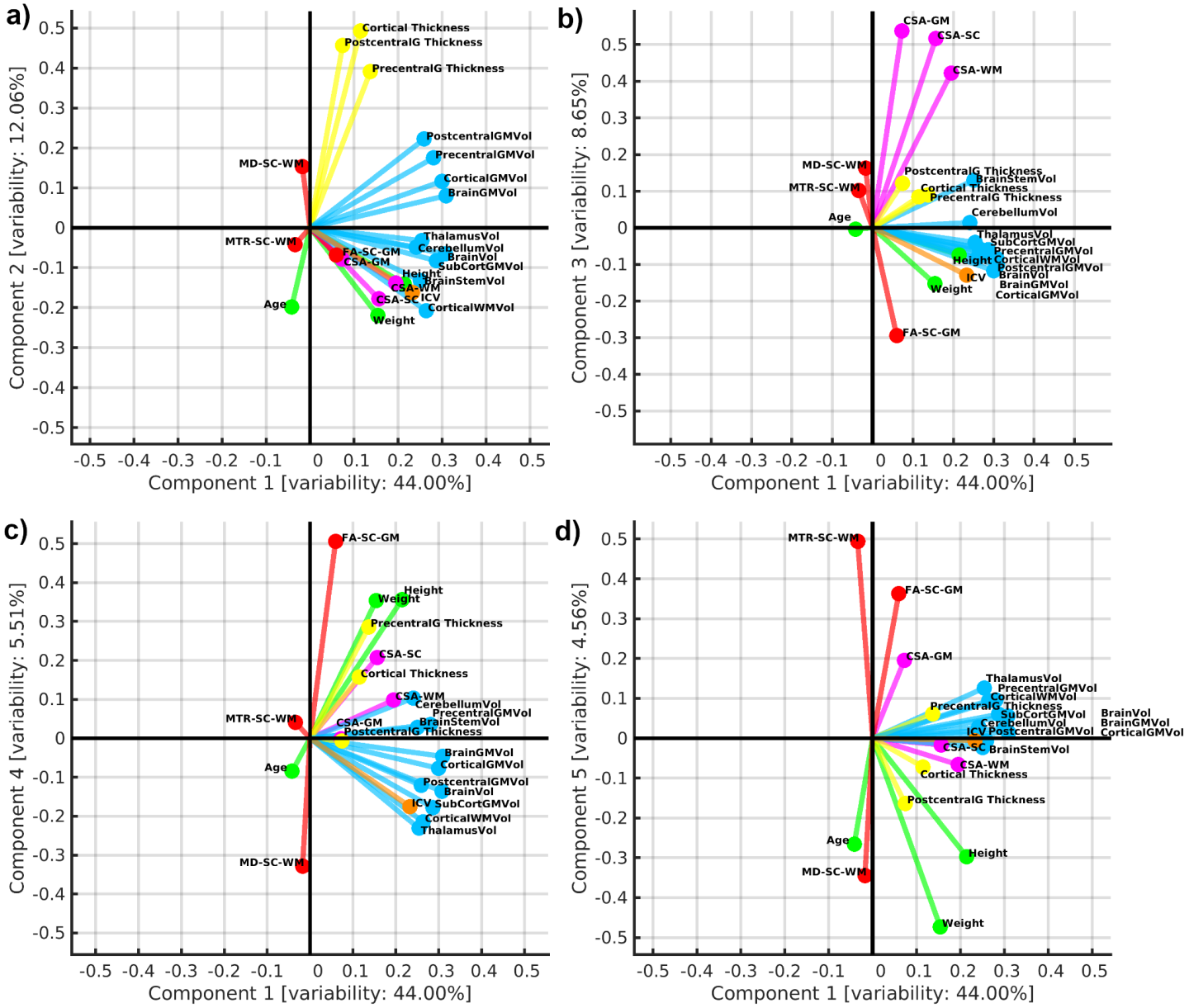

Figure 7: Exploratory visualization using biplot projections of principal components.
a) biplot projection of 1st and 2nd principal components (PCs); **b)** biplot projection of 1st and 3rd PCs; **c)** biplot projection of 1st and 4th PCs; **d)** biplot projection of 1st and 5th PCs. Variable vectors are visualized in each biplot projection with a color-coding characteristic for a corresponding variable group. Variable name abbreviations and variable color codings are described as follows. *Variable abbreviations:* ICV - intracranial volume; MD - mean diffusivity; RD - radial diffusivity; MTR - magnetization transfer ratio; SC - spinal cord; WM - white matter; GM - gray matter; CSA - cross-sectional area; Vol - volume; PrecentralG - precentral gyrus; PostcentralG - postcentral gyrus. *Variable color coding:* ICV - orange; demography - green; cerebral volumes - light blue; cortical thicknesses - yellow; SC morphometry - magenta; SC WM microstructure - red. *How to read a biplot:* The overall domain of each component axis is <-1,1>. Each variable is characterized as a vector of magnitude in the range of <0,1> in the biplot space. Angle 0° between the component axis and variable vector with magnitude 1 (or between two variable vectors both with magnitude 1) is proportional to Pearson correlation coefficient 1. Under the same vector magnitude circumstances, an angle of 180° equals Pearson correlation coefficient -1, and angles of 90° and 270° equal Pearson correlation coefficient 0. The lower magnitude of variable vectors proportionally decreases the overall linear dependence between vector angles close to 0° or 180°, respectively. Similarly, angle deviation from 0° or 180° also decreases the level of linear dependence between pairs of vectors in the biplot.

4 Discussion

The current study, using the *spine-generic* dataset, presents unique multi-center in vivo evidence about adult human cervical SC and brain, and emphasizes the following findings:

(i) Body height correlates moderately with SC WM and brain morphology, improves explanation of demography-related variance in such structural measurements from 26±10% (range 6-37%) to 33±11% (range 12-46%) in young adults, and underlines the impact of such pathology unrelated variability in structural neuroimaging data. When ICV is added into the morphology modeling, the explained variance increases to 46±17% (range 16-69%).

(ii) The expected aging effects (Bédard & Cohen-Adad, 2022; Fjell et al., 2013; Heymsfield et al., 2009; Papinutto et al., 2020; Peters, 2006; Thambisetty et al., 2010) explain minimal amounts of SC and brain structural data variance (2±2%) in young adults except cortical thickness (8%).

(iii) Body height predominantly impacts cortical GM volume (**Fig. 2b**) and may even define overall brain GM volume.

(iv) Body weight correlates weakly with SC WM MTR, which is influenced by myelin content.

(v) Body weight correlates weakly with SC WM microstructure assessed with DTI MD.

(vi) Body weight explains ≈5-7% of DTI and MTR data variance.

(vii) SC WM DTI and MTR explain a significant portion of examined dataset variance (≈14-19%) and are nearly orthogonal to most macrostructural measurements, except for the CSA-GM.

(viii) Subcortical and cortical GM volumes are correlated with CSA-WM more profoundly than the cerebellar volume with a descending correlation gradient from the brainstem toward cortical GM (**Fig. 2c**).

(ix) Cortical WM, subcortical GM, and brainstem volumes correlate with CSA-GM but much less profoundly than CSA-WM.

(x) Cortical thickness of the precentral cortex correlates weakly with CSA-WM.

(xi) We highlight the importance of considering the scanner-related effects present in SC imaging data (Cohen-Adad et al., 2021a, 2021b).

(xii) We confirm significant relationships between body size, brain volumes/weight, and CSA-SC in line with previously reported results (Baaré et al., 2001; Bédard & Cohen-Adad, 2022; Kameyama et al., 1994).

(xiii) We confirmed strong ICV effects on brain morphology (Miller et al., 2016). Moreover, we demonstrated interactions between ICV and CSA-WM and that utilizing both ICV and body height can maximize the amount of explained variance in CNS morphology (i.e., brain volumetry and CSA measurements in the spinal cord).

(xiv) We showed that ICV normalization of brain volumes amplifies ICV-related variance/entropy in all tested regions of interest. Moreover, the normalization emphasized scanner effects.

(xv) Females showed a consistently lower level of association with the variables of interest compared to males; and thus also a lower predictive power of the tested linear mixture models to the brain and SC morphology.

4.1 Practical impact of the current study in clinical neuroimaging study designs

MRI of SC structure is emerging in clinical research of neurodegenerative diseases and SC injuries (Badhiwala et al., 2020; David et al., 2019; de Albuquerque et al., 2017; Fatemi et al., 2005; Hernandez et al., 2022; Huffnagel et al., 2019; Lema et al., 2017; Lukas et al., 2013; Pisharady et al., 2020; Querin et al., 2017; Schmierer et al., 2004; van de Stadt et al., 2020). Microstructural SC MRI of neural tissue integrity aims to understand pathophysiological changes at the subclinical or presymptomatic stage (Joers et al., 2022; Labounek et al., 2020; Martin et al., 2018; Valošek et al., 2021). Quantitative MRI has made significant advances over the past two decades for brain imaging (Ahn et al., 2019; Anik et al., 2007; Appelman et al., 2009; Asken et al., 2018; Aylward et al., 2000; Benatar et al., 2022; Fox et al., 1996; Ginestroni et al., 2009; Hall et al., 2008; Hayakawa et al., 2013; Kabani et al., 2002; Kinnunen et al., 2018; Masuda et al., 2022; Reading et al., 2005; Ringman et al., 2007; Rosano et al., 2005, 2010; Rosas et al., 2006; Rovira et al., 2001; Wade et al., 2008), but is still in its early development stage when it comes to SC imaging. Sex- and

age-matching are critical for any clinical neuroimaging study. Yet, we are proposing that mismatched variability in body size may influence imaging outcomes more profoundly than mismatched variability in age. Persistent marginal impact of body stature on brain structural and functional neuroimaging outcomes in the early elderly population (Alfaro-Almagro et al., 2021; Miller et al., 2016) further underlines the importance of our proposal. Therefore, body size needs to be considered in the rigor of future neuroimaging studies focusing on between-group differences in brain or SC structure to secure and guarantee the reproducibility of results. It has not been a common practice in design of the vast majority of current clinical studies focusing on brain or SC neuroimaging. An alternative solution in future clinical study designs can be normalizing structural measurements for body size or using body size as a confounding factor. In brain volume measurements, e.g., SIENAX (Smith et al., 2002) or other kinds of normalization for the total ICV may offer an effective normalization method that provides reproducible results independent of body size. In the SC morphology, SIENAX (Papinutto et al., 2020) or the dimension of pontomedullary junction (Bédard & Cohen-Adad, 2022) have been implemented to normalize the CSA measurement. Yet, if possible, we conclude that body size matching provides a more optimal study design solution because we showed that body size characterizes a significant portion of CNS structural information that is not characterized by the ICV. Simultaneously, recruitment of body size matched participants should be an easier clinical design task than to utilize ICV matching.

4.2 Body size, sex, neuroimaging and CNS (patho-)physiology

Body height had the highest impact on brain GM and SC WM morphology. Body height, higher cortical volume, and improved cognitive ability appears to be phenotypically interlinked (Vuoksimaa et al., 2018). The higher brain GM volumes in taller people may also explain their higher resistance to Alzheimer's disease and other dementias (Daghlas et al., 2023; Jørgensen et al., 2020; Larsson et al., 2017). Gene expression could play a role here, as genetic variants that affect height also influence brain development and biological pathways that are involved in the development of Alzheimer's disease (Larsson et al., 2017).

Although our data showed an insignificant interaction between body weight and CNS morphology after controlling for sex, body weight is known to influence CNS morphology and microstructure. Varying body weight showed WM and GM brain volume loss in patients with acute anorexia nervosa, and full WM volume and almost complete GM volume recoveries after the body weight had been regained (Seitz et al., 2014). In the opposite body weight spectrum, obesity demonstrated lower intra-cortical myelination in regions involved in reward processing, attention, salience detection, and higher intra-cortical myelination in regions associated with somatosensory processing and inhibitory control (Dong et al., 2021). High cumulative BMI is associated with smaller brain volume, larger volume of white matter lesions, and abnormal microstructural integrity (Lv et al., 2024; Ward et al., 2005; West et al., 2020). Increasing BMI changes cerebral WM microstructure assessed with DTI (Kullmann et al., 2016), but direction of DTI parameter trends in relation to body weight varies between studies (Okudzhava et al., 2022). Although precise pathophysiological processes are not well known today, it is certain that obesity causes neuroinflammation, thus, alters brain microstructure and increases risks of neurodegenerative disorders such as Alzheimer's disease and other types of dementias (Woo et al., 2022). Our DTI and MTR data acquired in the current healthy population with low-to-moderate BMI may point to a borderline trend between homeostasis and mild microstructural changes related to higher body weight. The negative correlation between body weight and MTR has also recently been reported in peripheral nerves and skeletal muscles (Fösleitner et al., 2022). However, we cannot rule out the possibility of a transmit field (i.e., B1+) inhomogeneity-mediated bias in MTR. Although B1+ maps were not measured for the cervical SC in our study, similar to what has been observed in the brain at 3T (Glasser et al., 2022), we expect both B1+ inhomogeneity and deviation to correlate with body weight positively, hence body transmit coil loading. Typically, an underflipping (i.e., reaching smaller than the desired flip angle) is more likely than an overflipping for small structures like the cervical SC in the body. MTR's sensitivity to B1+ potentially exacerbates the effect of even a small degree of underflipping for the MT pulse at 3T.

Body height and spinal cord length are linearly dependent (r≈0.6) (Fradet et al., 2014; Zyoud et al., 2020). We showed that even CSA-SC and CSA-WM are linearly dependent with body height. Thus, the magnitude of the correlation with body height would be even higher than observed for the CSA measurements if level-specific SC and SC WM volumes were analyzed. Although CSA values are level dependent (Cohen-Adad et al., 2021a), the impact of the C3-4 level selection on general study conclusions should remain minimal due to high intra-individual CSA correlation over segments (Healy et al., 2012; Kameyama et al., 1996). Different associations of CSA-GM and CSA-WM with other investigated variables may affirm the necessity of further development of MRI protocols imaging SC GM in high contrast and detail (Cohen-Adad et al., 2022).

Recently, the correlation between CSA-SC at C2-3 level and body height, body weight, brain (WM/GM) volumes and thalamus volume were observed in 804 UK Biobank brain imaging database participants (Bédard & Cohen-Adad, 2022). Our current *spine-generic* database study complements the UK Biobank results and expands the knowledge that these observations are almost exclusively SC WM-related. Moreover, the current study identified more cerebral sub-regions involved than those investigated in the previous study. The lateral corticospinal tracts predominantly serving motor function are the major portion of the CSA-WM (Chandar & Freeman, 2014). Thus, its significant correlation with precentral gyrus thickness (primary motor cortex) seems logical from a neuroanatomical perspective. SC microstructure was also investigated and our exploratory approach via PCA clearly visualizes the body-SC-brain structural relationships.

Although we showed interactions between CSA-WM and ICV and that ICV can explain variance in SC morphology, it can often be challenging to design a neuroimaging study that measures both parameters. Studies focusing on SC pathology do not often acquire brain images (David et al., 2019; Kadanka et al., 2017; Kerkovský et al., 2012; Labounek et al., 2020; Martin et al., 2017, 2018; Nouri et al., 2016; Valošek et al., 2021). In case of the ultra-high field MRI (≥7T), it can even be a challenging task as the highly optimized SC imaging coils do not cover the whole brain (Lopez-Rios et al., 2023).

Although clinical studies focusing on cerebral atrophy often normalize distinct brain region volumes with ICV (Voevodskaya et al., 2014; Whitwell et al., 2001; Xie et al., 2005) and we would usually normalize the data too, our cross-sectional results suggest that the normalization magnifies ICV information in such volume measurements. The ICV normalization impact on associations with neurocognitive or behavioral outcomes remains unclear. ICV normalization flips signs of the association with neurocognitive outcomes in dementia, but does not change the overall association conclusion (Konstantinou et al., 2016; Wang et al., 2024). The opposite sign may be an effect of the additional ICV^{-1} scaling factor. However, ICV normalization biases volume-based behavioral models (Dhamala et al., 2022). In the *spine-generic* dataset, the Freesurfer provided higher BrainSegVol (brain volume) than eITV (ICV) in 18 scans. The FreeSurfer was reported to overestimate ICV by about 4% due to brain volume bias (Klasson et al., 2018), but that does not explain our observed phenomena that BrainSegVol can be higher than eITV. Future research may assess brain volume and ICV with concurrent tools (Harkey et al., 2022; Manjón & Coupé, 2016; Nerland et al., 2022).

The slightly lower variance in female data may be a cause of the lower predictive power of the utilized linear mixture models to brain and SC morphology. However, we doubt that it would halve the predictive accuracy. Thus, we speculate that unidentified female-specific biological factor(s) further determine females' CNS morphology. Brain structural organization differs between males and females, potentially due to different hormonal levels and gene expression (Liu et al., 2020). Moreover, a pregnancy increases hormone production and induces long-lasting reversible and irreversible changes in females' brain structure (Hoekzema et al., 2017; Pritschet et al., 2024). Neither hormonal, genetic and pregnancy data were collected thus impossible to test in the models with the current *spine-generic* records.

The *spine-generic* database (*r20231212*) identifies 64 recruited subjects with the presence of degenerative cervical SC compression, with 2 of these even demonstrating radiological signs of myelopathy (Valošek et al., 2024). These findings may represent a source of unexplained variance in our results, as compression and

myelopathy are pathologies affecting CSA, DTI, and MTR measures (Kadanka et al., 2017; Labounek et al., 2020; Martin et al., 2018; Valošek et al., 2021). However, we showed in the **Supplementary Slides** that the impact of the compression on the correlation coefficient outcomes was minimal.

The observed negative correlation between age and cortical thickness and absence of correlation between body size and cortical thickness are in line with previous literature (Frangou et al., 2022; Sowell et al., 2007; Tamnes et al., 2010; Thambisetty et al., 2010; Vuoksimaa et al., 2018). The GM volume reduction in subcortical structures is less profound than in the cortical GM volume and thickness (Fjell et al., 2013, 2021; Narvacan et al., 2017). Therefore, we may only detect low, insignificant trends in the age-related reductions of the subcortical structures due to an undersampled elderly population in our dataset. SC CSA-GM is also expected to decline with age (Papinutto et al., 2015), but we observed no such effects. Absent SC GM reduction might imply a false positive result due to the limited spatial resolution of the imaging methods, and the undersampled elderly population. It may also mean that the pathophysiological dynamics of SC GM reduction are slower than in the subcortical region. Yet, validating and concluding any of such statements require a rigorous re-test utilizing a dataset with a larger sample elderly population or longitudinal follow-up.

4.3 Study limitations

Despite the relatively large sample size, there are still several limitations. First, we recruited healthy, predominantly young adults with average weight and low-to-moderate BMI. Therefore, the negative link between age and SC morphology, as observable in cohorts with greater age variability (Bédard & Cohen-Adad, 2022; Ishikawa et al., 2003; Papinutto et al., 2015), was absent in our study. We found that body size impacts structural measurements more profoundly than age. However, this finding warrants further investigation, as the moderate age effects may be explained by the relatively narrow age range and younger cohort (Heymsfield et al., 2009). However, concurrent study of 40-69-year-old adults also showed significant impact of body size on brain neuroimaging data (Alfaro-Almagro et al., 2021; Miller et al., 2016). ICV and head size were identified as an effective confounding factor minimizing the body size effects in brain structural measurements (Alfaro-Almagro et al., 2021; Miller et al., 2016). The head size is not possible to measure precisely from the *spine-generic* database, because the images covering the brain were manually defaced by deleting the facial area in images. Thus, a significant portion of the image capturing head is missing in every scan. Yet, we employed the ICV covariate that is highly correlated to the head size and expected to be a more relevant measure for brain-related analyses (Miller et al., 2016). CSA-GM, SC DTI, and SC MTR measurements demonstrated scanner-related variability, which needs to be addressed in multi-center data acquisition and analysis. Data of subjects with very low and high BMI may help to investigate the dependence of MTR and DTI measures on body weight. RF inhomogeneities need to be better mapped in future studies to avoid risks of biases in MTR outcomes. Comparison between SC and cerebral microstructure is impossible with the *spine-generic* database because the database does not contain images of brain microstructure. The current *spine-generic* database version does not allow assessing the impact of socioeconomic and race/ethnicity status on obtained MRI metrics (Piccolo et al., 2016). Relationships between spinal canal area (Fradet et al., 2014), cervical cerebrospinal fluid area (Fradet et al., 2014), and body size have not been investigated. Axial diffusivity (AD, i.e., another DTI metric) was not investigated. We expected that AD would provide similar results as observed for MD and RD due to expected high FA-MD-RD-AD intra-correlation levels; therefore, we decided to shrink the variable space. Overall, we conclude that body height and weight should be sufficient and self-explanatory measures of body size for the current study outcomes. However, future studies should measure LBW more rigorously than has been possible here and determine LBW effects on CNS microstructure. Reliable interpretation and additional value of our LBW and BSA association results may be limited because they were theoretically calculated utilizing body height and weight. The cross-sectional study design limits testing of body size changes on the CNS over time.

5 Conclusions

(i) We confirmed that *"Future clinical research studies and trials utilizing neuroimaging should include body size as a potential confounding biological factor to avoid bias in clinical outcomes"*. ***(ii)*** We hypothesized that "CSA of cervical SC WM and GM interacts with body size and morphology of distinct brain structures", but after analysis we refine this to *"CSA of cervical SC WM interacts with body height and morphology of distinct brain structures with a descending gradient from subcortical structures to cortical gray matter"*. ***(iii)*** We hypothesized that "SC microstructure, as measured using MTR and DTI, interacts with body size", but after analysis we refine this to *"SC WM microstructure, as measured as MD and MTR, interacts with body weight, and more profoundly in dorsal columns than in lateral corticospinal tracts"*. We confirmed our hypotheses that ***(iv)*** *"Cerebral morphology interacts with body height more profoundly than with body weight and age"*; and that ***(v)*** *"Body size increases the predictive power of CNS structure"*.

6 Data and Code Availability

All raw data are publicly available at: https://github.com/spine-generic/data-multi-subject (utilized release ID: r20231212)

MRI imaging protocols for all optimized manufacturers and scanner types are publicly available at: https://github.com/spine-generic/protocols

Tables with SCT and Freesurfer measurements are available at: https://github.com/umn-milab/spine-generic-body-size-results (utilized release ID: r20250226)

Spinal Cord Toolbox is available at: https://github.com/spinalcordtoolbox/spinalcordtoolbox (utilized version: 6.1; git commit: git-master-c7a8072fd63a06a2775a74029c042833f0fce510)

FreeSurfer is available at: https://surfer.nmr.mgh.harvard.edu (utilized version: 7.2)

All computer code providing image and statistical analyses is available at: https://github.com/spine-generic/spine-generic (utilized release ID: height-weight-analysis-v1.2)

7 Author Contributions

RL initiated post-collection of missing demographic data, performed image analysis of spinal cord images and statistical analysis, designed figures and tables, and drafted the manuscript. MTB and ALP performed image analysis of brain images. EAO, SB, AF, JV and JCA provided data management and curation, and computer code integration into the *spine-generic* project. RL, SB, MA, EAO, NTA, LRB, RLB, MarBar, MarBat, CB, MDB, VC, AC, BDL, MDe, PLS, MDo, JD, AVD, FE, KRE, KSE, PF, JF, AF, MF, IF, CAMGW-K, GCG, GG, FeGi, FrGr, AH, P-GH, TH, MH, JMJ, KK, HK, MK, AK, J-WK, NK, HK, SK, YK, PeKu, PaKu, NDK, SK, MML, CoLa, CSWL, TL, YL, SL, SM, ARM, EM-H, LM, KPO'G, NP, DaPa, DePa, TBP, AP, FP, AR, MJR, RSS, GS, MS, ACS, AKS, SAS, ZAS, ES, YS, GT, AT, JV, DVDV, MCY, KAW II, NW, RGW, POW, JX, JCA, ChLe and IN collected data. JCA, ChLe and IN supervised RL, MTB and ALP in data analysis and substantially revised the first manuscript draft. *All authors* designed and conceptualized the study, read and revised the manuscript.

8 Funding

S Llufriu holds grants from the ISCIII [PI21/01189], AGAUR [021-SGR-01325] and research support from Bristol Myers Squibb. CWK receives funding from MRC (#MR/S026088/1), Ataxia UK, Rosetrees Trust (#PGL22/100041 and #PGL21/10079). The research reported in this publication was also supported by the *National Natural Science Foundation of China* (82072010); the *Beijing Natural Science Foundation* [IS23108];

the *Ministry of Health, Czech Republic* - conceptual development of research organization [FNBr, 65269705]; the *Ministry of Education, Youth and Sports, Czech Republic* [LM2018129 Czech-BioImaging], part of the *Euro-BioImaging* (www.eurobioimaging.eu) *Advanced Light Microscopy and Medical Imaging Node* (Brno, Czech Republic); the *Max Planck Society* and the *European Research Council* [ERC StG 758974, European Union's Horizon 2020 research and innovation programme 758974]; the *University of Pennsylvania* [MDBR-17-123-MPS - Million Dollar Bike Ride]; the *Instituto Salud Carlos III* - co-funded *European Union* [PI18/00823, PI22/01709]; the *Ministry of Health of the Czech Republic* [NU22-04-00024]; the *European Union's Horizon Europe* research and innovation programme under the Marie Skłodowska-Curie grant [101107932]; the *American Heart Association* [23CDA1054207]; the *Fondation Courtois*; the *Natural Sciences and Engineering Research Council of Canada* (NSERC), TransMedTech Institute, ICORD [RGPIN-2020–05242] and UBC; the *Craig H. Neilsen Foundation*; the *"la Caixa" Foundation* [ID 100010434; fellowship code LCF/BQ/PR22/11920010]; the *Wings For Life charity* [WFL-CH-19/20]; the *International Foundation for Research* [IRP-158]; the *Czech Health Research Council* [NV18-04-00159]; the *National Institute for Health Research Biomedical Research Centre at UCL and UCLH*; the *German Research Foundation* [TI 1110/1-1]; the *SpinalCure Australia*; the BRC [BRC1130/HEI/RS/11041]; the *European Union - NextGenerationEU* under the *Italian Ministry of University and Research (MUR) National Innovation Ecosystem* [ECS00000041 - VITALITY - CUP D73C22000840006]; the *Canada Research Chair in Quantitative Magnetic Resonance Imaging* [CRC-2020-00179]; the *Canadian Institute of Health Research* [PJT-190258]; the *Canada Foundation for Innovation* [32454, 34824]; the *Fonds de Recherche du Québec - Santé* [322736, 324636]; the *Natural Sciences and Engineering Research Council of Canada* [RGPIN-2019-07244]; the *Canada First Research Excellence Fund* (IVADO and TransMedTech), the *Courtois NeuroMod project*; the *Quebec BioImaging Network* [5886, 35450]; the *INSPIRED* (Spinal Research, UK; Wings for Life, Austria; Craig H. Neilsen Foundation, USA); the *Mila - Tech Transfer Funding Program*; and the *National Institutes of Health* (NIH) through the National Institute of Neurological Disorders and Stroke and the National Institute of Biomedical Imaging and Bioengineering [P41EB027061, P30NS076408, K23NS104211, L30NS108301, R01NS128478, R01NS133305, K01NS105160, K01EB030039, 5R01NS109114, K24NS126781, R61NS118651, R00EB016689, R01EB027779, R21EB031211, R01NS109450, and R03NS139000]. The content is solely the responsibility of the authors and does not necessarily represent the official views of the NIH.

9 Declaration of Competing Interests

Since June 2022, Dr. A.K. Smith has been employed by GE HealthCare. This article was co-authored by Dr. Smith in his personal capacity. The opinions expressed in the article are his in and do not necessarily reflect the views of GE HealthCare.

Since August 2022, Dr. M. M. Laganà has been employed by Canon Medical Systems srl, Rome, Italy. This article was co-authored by Dr. M. M. Laganà in her personal capacity. The opinions expressed in the article are her own and do not necessarily reflect the views of Canon Medical Systems.

Since September 2023, Dr. Papp has been an employee of Siemens Healthcare AB, Sweden. This article was co-authored by Dr. Papp in his personal capacity. The views and opinions expressed in this article are his own and do not necessarily reflect the views of Siemens Healthcare AB, or Siemens Healthineers AG.

Since January 2024, Dr. Barry has been employed by the National Institute of Biomedical Imaging and Bioengineering at the NIH. This article was co-authored by Robert Barry in his personal capacity. The opinions expressed in the article are his own and do not necessarily reflect the views of the NIH, the Department of Health and Human Services, or the United States government.

Guillaume Gilbert is an employee of Philips Healthcare.

S Llufriu received compensation for consulting services and speaker honoraria from Biogen Idec, Novartis, Bristol Myer Squibb Genzyme, Sanofi Jansen and Merck.

The Max Planck Institute for Human Cognitive and Brain Sciences and Wellcome Centre for Human Neuroimaging have institutional research agreements with Siemens Healthcare. NW holds a patent on acquisition of MRI data during spoiler gradients (US 10,401,453 B2). NW was a speaker at an event organized by Siemens Healthcare and was reimbursed for the travel expenses.

CGWK is a shareholder in Queen Square Analytics Ltd.

The other authors declare no competing interests.

10 Acknowledgments

The Center for Magnetic Resonance Research (CMRR), Department of Radiology; the Center for Neurobehavioral Development (CNBD) at the Masonic Institute for the Developing Brain (MIDB), Department of Pediatrics; and the Minnesota Supercomputing Institute (MSI); all are part of the University of Minnesota and all provided lab space and computational support for this research project. The authors acknowledge the facilities, scientific and technical assistance of the National Imaging Facility, a National Collaborative Research Infrastructure Strategy (NCRIS) capability, at the Centre for Advanced Imaging, The University of Queensland. This work is based on experiments performed at the Swiss Center for Musculoskeletal Imaging, SCMI, Balgrist Campus AG, Zurich.

11 References

Aboitiz, F., Scheibel, A. B., Fisher, R. S., & Zaidel, E. (1992). Fiber composition of the human corpus callosum. *Brain Research*, *598*(1-2), 143–153. https://doi.org/10.1016/0006-8993(92)90178-c

Ahn, J. H., Kim, M., Kim, J. S., Youn, J., Jang, W., Oh, E., Lee, P. H., Koh, S.-B., Ahn, T.-B., & Cho, J. W. (2019). Midbrain atrophy in patients with presymptomatic progressive supranuclear palsy-Richardson's syndrome. *Parkinsonism & Related Disorders*, *66*, 80–86. https://doi.org/10.1016/j.parkreldis.2019.07.009

Alfaro-Almagro, F., Jenkinson, M., Bangerter, N. K., Andersson, J. L. R., Griffanti, L., Douaud, G., Sotiropoulos, S. N., Jbabdi, S., Hernandez-Fernandez, M., Vallee, E., Vidaurre, D., Webster, M., McCarthy, P., Rorden, C., Daducci, A., Alexander, D. C., Zhang, H., Dragonu, I., Matthews, P. M., … Smith, S. M. (2018). Image processing and Quality Control for the first 10,000 brain imaging datasets from UK Biobank. *NeuroImage*, *166*, 400–424. https://doi.org/10.1016/j.neuroimage.2017.10.034

Alfaro-Almagro, F., McCarthy, P., Afyouni, S., Andersson, J. L. R., Bastiani, M., Miller, K. L., Nichols, T. E., & Smith, S. M. (2021). Confound modelling in UK Biobank brain imaging. *NeuroImage*, *224*, 117002. https://doi.org/10.1016/j.neuroimage.2020.117002

Anik, Y., Iseri, P., Demirci, A., Komsuoglu, S., & Inan, N. (2007). Magnetization transfer ratio in early period of Parkinson disease. *Academic Radiology*, *14*(2), 189–192. https://doi.org/10.1016/j.acra.2006.11.005

Appelman, A. P. A., Exalto, L. G., van der Graaf, Y., Biessels, G. J., Mali, W. P. T. M., & Geerlings, M. I. (2009). White matter lesions and brain atrophy: more than shared risk factors? A systematic review. *Cerebrovascular Diseases* , *28*(3), 227–242. https://doi.org/10.1159/000226774

Asken, B. M., DeKosky, S. T., Clugston, J. R., Jaffee, M. S., & Bauer, R. M. (2018). Diffusion tensor imaging (DTI) findings in adult civilian, military, and sport-related mild traumatic brain injury (mTBI): a systematic critical review. *Brain Imaging and Behavior*, *12*(2), 585–612. https://doi.org/10.1007/s11682-017-9708-9

Aylward, E. H., Codori, A. M., Rosenblatt, A., Sherr, M., Brandt, J., Stine, O. C., Barta, P. E., Pearlson, G. D., & Ross, C. A. (2000). Rate of caudate atrophy in presymptomatic and symptomatic stages of Huntington's disease. *Movement Disorders: Official Journal of the Movement Disorder Society*, *15*(3), 552–560. https://doi.org/10.1002/1531-8257(200005)15:3<552::AID-MDS1020>3.0.CO;2-P

Baaré, W. F., Hulshoff Pol, H. E., Boomsma, D. I., Posthuma, D., de Geus, E. J., Schnack, H. G., van Haren, N. E., van Oel, C. J., & Kahn, R. S. (2001). Quantitative genetic modeling of variation in human brain morphology. *Cerebral Cortex* , *11*(9), 816–824. https://doi.org/10.1093/cercor/11.9.816

Badhiwala, J. H., Ahuja, C. S., Akbar, M. A., Witiw, C. D., Nassiri, F., Furlan, J. C., Curt, A., Wilson, J. R., & Fehlings, M. G. (2020). Degenerative cervical myelopathy — update and future directions. In *Nature Reviews Neurology* (Vol. 16, Issue 2, pp. 108–124). https://doi.org/10.1038/s41582-019-0303-0

Battaglini, M., Jenkinson, M., & De Stefano, N. (2012). Evaluating and reducing the impact of white matter lesions on brain volume measurements. *Human Brain Mapping*, *33*(9), 2062–2071. https://doi.org/10.1002/hbm.21344

Bédard, S., & Cohen-Adad, J. (2022). Automatic measure and normalization of spinal cord cross-sectional area using the pontomedullary junction. *Frontiers in Neuroimaging*, *1*. https://doi.org/10.3389/fnimg.2022.1031253

Benatar, M., Wuu, J., McHutchison, C., Postuma, R. B., Boeve, B. F., Petersen, R., Ross, C. A., Rosen, H., Arias, J. J., Fradette, S., McDermott, M. P., Shefner, J., Stanislaw, C., Abrahams, S., Cosentino, S., Andersen, P. M., Finkel, R. S., Granit, V., Grignon, A.-L., … First International Pre-Symptomatic ALS Workshop. (2022). Preventing amyotrophic lateral sclerosis: insights from pre-symptomatic neurodegenerative diseases. *Brain: A Journal of Neurology*, *145*(1), 27–44. https://doi.org/10.1093/brain/awab404

Boesch, S. M., & Indelicato, E. (2021). Body Mass Index and Height in Friedreich Ataxia: What Do We Know? *Neurology. Genetics*, *7*(6), e637. https://doi.org/10.1212/NXG.0000000000000637

Butler, M. G., Miller, B. S., Romano, A., Ross, J., Abuzzahab, M. J., Backeljauw, P., Bamba, V., Bhangoo, A., Mauras, N., & Geffner, M. (2022). Genetic conditions of short stature: A review of three classic examples. *Frontiers in Endocrinology*, *13*, 1011960. https://doi.org/10.3389/fendo.2022.1011960

Callaghan, M. F., Freund, P., Draganski, B., Anderson, E., Cappelletti, M., Chowdhury, R., Diedrichsen, J., Fitzgerald, T. H. B., Smittenaar, P., Helms, G., Lutti, A., & Weiskopf, N. (2014). Widespread age-related differences in the human brain microstructure revealed by quantitative magnetic resonance imaging. *Neurobiology of Aging*, *35*(8), 1862–1872. https://doi.org/10.1016/j.neurobiolaging.2014.02.008

Chandar, K., & Freeman, B. K. (2014). Spinal Cord Anatomy. In M. J. Aminoff & R. B. Daroff (Eds.), *Encyclopedia of the Neurological Sciences (Second Edition)* (pp. 254–263). Academic Press. https://doi.org/10.1016/B978-0-12-385157-4.01176-3

Cohen-Adad, J., Alonso-Ortiz, E., Abramovic, M., Arneitz, C., Atcheson, N., Barlow, L., Barry, R. L., Barth, M., Battiston, M., Büchel, C., Budde, M., Callot, V., Combes, A. J. E., De Leener, B., Descoteaux, M., de Sousa, P. L., Dostál, M., Doyon, J., Dvorak, A., … Xu, J. (2021a). Generic acquisition protocol for quantitative MRI of the spinal cord. *Nature Protocols*, *16*(10), 4611–4632. https://doi.org/10.1038/s41596-021-00588-0

Cohen-Adad, J., Alonso-Ortiz, E., Abramovic, M., Arneitz, C., Atcheson, N., Barlow, L., Barry, R. L., Barth, M., Battiston, M., Büchel, C., Budde, M., Callot, V., Combes, A. J. E., De Leener, B., Descoteaux, M., de Sousa, P. L., Dostál, M., Doyon, J., Dvorak, A., … Xu, J. (2021b). Open-access quantitative MRI data of the spinal cord and reproducibility across participants, sites and manufacturers. *Scientific Data*, *8*(1), 219. https://doi.org/10.1038/s41597-021-01044-0

Cohen-Adad, J., Alonso-Ortiz, E., Alley, S., Lagana, M. M., Baglio, F., Vannesjo, S. J., Karbasforoushan, H., Seif, M., Seifert, A. C., Xu, J., Kim, J.-W., Labounek, R., Vojtíšek, L., Dostál, M., Valošek, J., Samson, R. S., Grussu, F., Battiston, M., Gandini Wheeler-Kingshott, C. A. M., … Prados, F. (2022). Comparison of multicenter MRI protocols for visualizing the spinal cord gray matter. *Magnetic Resonance in Medicine: Official Journal of the Society of Magnetic Resonance in Medicine / Society of Magnetic Resonance in Medicine*. https://doi.org/10.1002/mrm.29249

Cox, R. W. (1996). AFNI: software for analysis and visualization of functional magnetic resonance neuroimages. *Computers and Biomedical Research, an International Journal*, *29*(3), 162–173. https://doi.org/10.1006/cbmr.1996.0014

Daghlas, I., Nassan, M., & Gill, D. (2023). Genetically proxied lean mass and risk of Alzheimer's disease: mendelian randomisation study. *BMJ Medicine*, *2*(1), e000354. https://doi.org/10.1136/bmjmed-2022-000354

David, G., Mohammadi, S., Martin, A. R., Cohen-Adad, J., Weiskopf, N., Thompson, A., & Freund, P. (2019). Traumatic and nontraumatic spinal cord injury: pathological insights from neuroimaging. *Nature Reviews. Neurology*, *15*(12), 718–731. https://doi.org/10.1038/s41582-019-0270-5

de Albuquerque, M., Branco, L. M. T., Rezende, T. J. R., de Andrade, H. M. T., Nucci, A., & França, M. C., Jr. (2017). Longitudinal evaluation of cerebral and spinal cord damage in Amyotrophic Lateral Sclerosis. *NeuroImage. Clinical*, *14*, 269–276. https://doi.org/10.1016/j.nicl.2017.01.024

De Leener, B., Lévy, S., Dupont, S. M., Fonov, V. S., Stikov, N., Louis Collins, D., Callot, V., & Cohen-Adad, J.

(2017). SCT: Spinal Cord Toolbox, an open-source software for processing spinal cord MRI data. *NeuroImage*, *145*(Pt A), 24–43. https://doi.org/10.1016/j.neuroimage.2016.10.009

Dhamala, E., Ooi, L. Q. R., Chen, J., Kong, R., Anderson, K. M., Chin, R., Yeo, B. T. T., & Holmes, A. J. (2022). Proportional intracranial volume correction differentially biases behavioral predictions across neuroanatomical features, sexes, and development. *NeuroImage*, *260*(119485), 119485. https://doi.org/10.1016/j.neuroimage.2022.119485

Dong, D., Wang, Y., Long, Z., Jackson, T., Chang, X., Zhou, F., & Chen, H. (2021). The Association between Body Mass Index and Intra-Cortical Myelin: Findings from the Human Connectome Project. *Nutrients*, *13*(9). https://doi.org/10.3390/nu13093221

Du Bois, D., & Du Bois, E. F. (1989). A formula to estimate the approximate surface area if height and weight be known. 1916. *Nutrition* , *5*(5), 303–311; discussion 312–313. https://www.ncbi.nlm.nih.gov/pubmed/2520314

Duval, T., Saliani, A., Nami, H., Nanci, A., Stikov, N., Leblond, H., & Cohen-Adad, J. (2019). Axons morphometry in the human spinal cord. *NeuroImage*, *185*, 119–128. https://doi.org/10.1016/j.neuroimage.2018.10.033

Engl, C., Schmidt, P., Arsic, M., Boucard, C. C., Biberacher, V., Röttinger, M., Etgen, T., Nunnemann, S., Koutsouleris, N., Reiser, M., Meisenzahl, E. M., & Mühlau, M. (2013). Brain size and white matter content of cerebrospinal tracts determine the upper cervical cord area: evidence from structural brain MRI. *Neuroradiology*, *55*(8), 963–970. https://doi.org/10.1007/s00234-013-1204-3

Fatemi, A., Smith, S. A., Dubey, P., Zackowski, K. M., Bastian, A. J., van Zijl, P. C., Moser, H. W., Raymond, G. V., & Golay, X. (2005). Magnetization transfer MRI demonstrates spinal cord abnormalities in adrenomyeloneuropathy. *Neurology*, *64*(10), 1739–1745. https://doi.org/10.1212/01.WNL.0000164458.02141.06

Fischl, B. (2012). FreeSurfer. *NeuroImage*, *62*(2), 774–781. https://doi.org/10.1016/j.neuroimage.2012.01.021

Fjell, A. M., Grydeland, H., Wang, Y., Amlien, I. K., Bartres-Faz, D., Brandmaier, A. M., Düzel, S., Elman, J., Franz, C. E., Håberg, A. K., Kietzmann, T. C., Kievit, R. A., Kremen, W. S., Krogsrud, S. K., Kühn, S., Lindenberger, U., Macía, D., Mowinckel, A. M., Nyberg, L., … Walhovd, K. B. (2021). The genetic organization of longitudinal subcortical volumetric change is stable throughout the lifespan. *eLife*, *10*. https://doi.org/10.7554/eLife.66466

Fjell, A. M., Westlye, L. T., Grydeland, H., Amlien, I., Espeseth, T., Reinvang, I., Raz, N., Holland, D., Dale, A. M., Walhovd, K. B., & Alzheimer Disease Neuroimaging Initiative. (2013). Critical ages in the life course of the adult brain: nonlinear subcortical aging. *Neurobiology of Aging*, *34*(10), 2239–2247. https://doi.org/10.1016/j.neurobiolaging.2013.04.006

Fösleitner, O., Schwehr, V., Godel, T., Preisner, F., Bäumer, P., Heiland, S., Bendszus, M., & Kronlage, M. (2022). Magnetization Transfer Ratio of Peripheral Nerve and Skeletal Muscle. *Clinical Neuroradiology*, *32*(2), 557–564. https://doi.org/10.1007/s00062-021-01067-5

Fox, N. C., Warrington, E. K., Freeborough, P. A., Hartikainen, P., Kennedy, A. M., Stevens, J. M., & Rossor, M. N. (1996). Presymptomatic hippocampal atrophy in Alzheimer's disease. A longitudinal MRI study. *Brain: A Journal of Neurology*, *119 (Pt 6)*, 2001–2007. https://doi.org/10.1093/brain/119.6.2001

Fradet, L., Arnoux, P.-J., Ranjeva, J.-P., Petit, Y., & Callot, V. (2014). Morphometrics of the entire human spinal cord and spinal canal measured from in vivo high-resolution anatomical magnetic resonance imaging. *Spine*, *39*(4), E262–E269. https://doi.org/10.1097/BRS.0000000000000125

Frangou, S., Modabbernia, A., Williams, S. C. R., Papachristou, E., Doucet, G. E., Agartz, I., Aghajani, M., Akudjedu, T. N., Albajes-Eizagirre, A., Alnaes, D., Alpert, K. I., Andersson, M., Andreasen, N. C., Andreassen, O. A., Asherson, P., Banaschewski, T., Bargallo, N., Baumeister, S., Baur-Streubel, R., … Dima, D. (2022). Cortical thickness across the lifespan: Data from 17,075 healthy individuals aged 3-90 years. *Human Brain Mapping*, *43*(1), 431–451. https://doi.org/10.1002/hbm.25364

Giedd, J. N., Snell, J. W., Lange, N., Rajapakse, J. C., Casey, B. J., Kozuch, P. L., Vaituzis, A. C., Vauss, Y. C., Hamburger, S. D., Kaysen, D., & Rapoport, J. L. (1996). Quantitative Magnetic Resonance Imaging of Human Brain Development: Ages 4–18. *Cerebral Cortex* , *6*(4), 551–559. https://doi.org/10.1093/cercor/6.4.551

Ginestroni, A., Battaglini, M., Della Nave, R., Moretti, M., Tessa, C., Giannelli, M., Caffarra, P., Nacmias, B., Bessi, V., Sorbi, S., Bracco, L., De Stefano, N., & Mascalchi, M. (2009). Early structural changes in individuals at risk of familial Alzheimer's disease: a volumetry and magnetization transfer MR imaging study. *Journal of Neurology*, *256*(6), 925–932. https://doi.org/10.1007/s00415-009-5044-3

Glasser, M. F., Coalson, T. S., Harms, M. P., Xu, J., Baum, G. L., Autio, J. A., Auerbach, E. J., Greve, D. N.,

Yacoub, E., Van Essen, D. C., Bock, N. A., & Hayashi, T. (2022). Empirical transmit field bias correction of T1w/T2w myelin maps. *NeuroImage*, *258*, 119360. https://doi.org/10.1016/j.neuroimage.2022.119360

Hall, A. M., Moore, R. Y., Lopez, O. L., Kuller, L., & Becker, J. T. (2008). Basal forebrain atrophy is a presymptomatic marker for Alzheimer's disease. *Alzheimer's & Dementia: The Journal of the Alzheimer's Association*, *4*(4), 271–279. https://doi.org/10.1016/j.jalz.2008.04.005

Harding, I. H., Chopra, S., Arrigoni, F., Boesch, S., Brunetti, A., Cocozza, S., Corben, L. A., Deistung, A., Delatycki, M., Diciotti, S., Dogan, I., Evangelisti, S., França, M. C., Jr, Göricke, S. L., Georgiou-Karistianis, N., Gramegna, L. L., Henry, P.-G., Hernandez-Castillo, C. R., Hutter, D., … Thompson, P. M. (2021). Brain structure and degeneration staging in friedreich ataxia: Magnetic resonance imaging volumetrics from the ENIGMA-ataxia working group. *Annals of Neurology*, *90*(4), 570–583. https://doi.org/10.1002/ana.26200

Harkey, T., Baker, D., Hagen, J., Scott, H., & Palys, V. (2022). Practical methods for segmentation and calculation of brain volume and intracranial volume: a guide and comparison. *Quantitative Imaging in Medicine and Surgery*, *12*(7), 3748–3761. https://doi.org/10.21037/qims-21-958

Hayakawa, Y. K., Sasaki, H., Takao, H., Mori, H., Hayashi, N., Kunimatsu, A., Aoki, S., & Ohtomo, K. (2013). Structural brain abnormalities in women with subclinical depression, as revealed by voxel-based morphometry and diffusion tensor imaging. *Journal of Affective Disorders*, *144*(3), 263–268. https://doi.org/10.1016/j.jad.2012.10.023

Healy, B. C., Arora, A., Hayden, D. L., Ceccarelli, A., Tauhid, S. S., Neema, M., & Bakshi, R. (2012). Approaches to normalization of spinal cord volume: application to multiple sclerosis. *Journal of Neuroimaging: Official Journal of the American Society of Neuroimaging*, *22*(3), e12–e19. https://doi.org/10.1111/j.1552-6569.2011.00629.x

Hernandez, A. L. C. C., Rezende, T. J. R., Martinez, A. R. M., de Brito, M. R., & França, M. C., Jr. (2022). Tract-specific spinal cord diffusion tensor imaging in Friedreich's ataxia. *Movement Disorders: Official Journal of the Movement Disorder Society*, *37*(2), 354–364. https://doi.org/10.1002/mds.28841

Heymsfield, S. B., Chirachariyavej, T., Rhyu, I. J., Roongpisuthipong, C., Heo, M., & Pietrobelli, A. (2009). Differences between brain mass and body weight scaling to height: potential mechanism of reduced mass-specific resting energy expenditure of taller adults. *Journal of Applied Physiology*, *106*(1), 40–48. https://doi.org/10.1152/japplphysiol.91123.2008

Hoekzema, E., Barba-Müller, E., Pozzobon, C., Picado, M., Lucco, F., García-García, D., Soliva, J. C., Tobeña, A., Desco, M., Crone, E. A., Ballesteros, A., Carmona, S., & Vilarroya, O. (2017). Pregnancy leads to long-lasting changes in human brain structure. *Nature Neuroscience*, *20*(2), 287–296. https://doi.org/10.1038/nn.4458

Huffnagel, I. C., van Ballegoij, W. J. C., Vos, J. M. B. W., Kemp, S., Caan, M. W. A., & Engelen, M. (2019). Longitudinal diffusion MRI as surrogate outcome measure for myelopathy in adrenoleukodystrophy. *Neurology*, *93*(23), e2133–e2143. https://doi.org/10.1212/WNL.0000000000008572

Ishikawa, M., Matsumoto, M., Fujimura, Y., Chiba, K., & Toyama, Y. (2003). Changes of cervical spinal cord and cervical spinal canal with age in asymptomatic subjects. *Spinal Cord*, *41*(3), 159–163. https://doi.org/10.1038/sj.sc.3101375

James, W. P. T. (1976). Research on obesity: A report of the DHSS/MRC group. In *For the Department of Health and Social Security and the Medical Research Council:* Her Majesty's Stationery Office.

Jenkinson, M., Beckmann, C. F., Behrens, T. E. J., Woolrich, M. W., & Smith, S. M. (2012). FSL. *NeuroImage*, *62*(2), 782–790. https://doi.org/10.1016/j.neuroimage.2011.09.015

Joers, J. M., Adanyeguh, I. M., Deelchand, D. K., Hutter, D. H., Eberly, L. E., Iltis, I., Bushara, K. O., Lenglet, C., & Henry, P.-G. (2022). Spinal cord magnetic resonance imaging and spectroscopy detect early-stage alterations and disease progression in Friedreich ataxia. *Brain Communications*, *4*(5), fcac246. https://doi.org/10.1093/braincomms/fcac246

Jørgensen, T. S. H., Okholm, G. T., Christensen, K., Sørensen, T. I., & Osler, M. (2020). Body height in young adult men and risk of dementia later in adult life. *eLife*, *9*. https://doi.org/10.7554/eLife.51168

Kabani, N. J., Sled, J. G., & Chertkow, H. (2002). Magnetization transfer ratio in mild cognitive impairment and dementia of Alzheimer's type. *NeuroImage*, *15*(3), 604–610. https://doi.org/10.1006/nimg.2001.0992

Kadanka, Z., Jr, Adamova, B., Kerkovsky, M., Kadanka, Z., Dusek, L., Jurova, B., Vlckova, E., & Bednarik, J. (2017). Predictors of symptomatic myelopathy in degenerative cervical spinal cord compression. *Brain and Behavior*, *7*(9), e00797. https://doi.org/10.1002/brb3.797

Kameyama, T., Hashizume, Y., Ando, T., & Takahashi, A. (1994). Morphometry of the normal cadaveric cervical spinal cord. *Spine*, *19*(18), 2077–2081. https://doi.org/10.1097/00007632-199409150-00013

Kameyama, T., Hashizume, Y., & Sobue, G. (1996). Morphologic features of the normal human cadaveric

spinal cord. *Spine*, *21*(11), 1285–1290. https://doi.org/10.1097/00007632-199606010-00001

Kerkovský, M., Bednarík, J., Dušek, L., Sprláková-Puková, A., Urbánek, I., Mechl, M., Válek, V., & Kadanka, Z. (2012). Magnetic resonance diffusion tensor imaging in patients with cervical spondylotic spinal cord compression: correlations between clinical and electrophysiological findings. *Spine*, *37*(1), 48–56. https://doi.org/10.1097/BRS.0b013e31820e6c35

Kinnunen, K. M., Cash, D. M., Poole, T., Frost, C., Benzinger, T. L. S., Ahsan, R. L., Leung, K. K., Cardoso, M. J., Modat, M., Malone, I. B., Morris, J. C., Bateman, R. J., Marcus, D. S., Goate, A., Salloway, S. P., Correia, S., Sperling, R. A., Chhatwal, J. P., Mayeux, R. P., … Dominantly Inherited Alzheimer Network (DIAN). (2018). Presymptomatic atrophy in autosomal dominant Alzheimer's disease: A serial magnetic resonance imaging study. *Alzheimer's & Dementia: The Journal of the Alzheimer's Association*, *14*(1), 43–53. https://doi.org/10.1016/j.jalz.2017.06.2268

Klasson, N., Olsson, E., Eckerström, C., Malmgren, H., & Wallin, A. (2018). Estimated intracranial volume from FreeSurfer is biased by total brain volume. *European Radiology Experimental*, *2*(1). https://doi.org/10.1186/s41747-018-0055-4

Konstantinou, N., Pettemeridou, E., Seimenis, I., Eracleous, E., Papacostas, S. S., Papanicolaou, A. C., & Constantinidou, F. (2016). Assessing the relationship between neurocognitive performance and brain volume in chronic moderate-severe traumatic brain injury. *Frontiers in Neurology*, *7*, 29. https://doi.org/10.3389/fneur.2016.00029

Kovac, V., Shapiro, E. G., Rudser, K. D., Mueller, B. A., Eisengart, J. B., Delaney, K. A., Ahmed, A., King, K. E., Yund, B. D., Cowan, M. J., Raiman, J., Mamak, E. G., Harmatz, P. R., Shankar, S. P., Ali, N., Cagle, S. R., Wozniak, J. R., Lim, K. O., Orchard, P. J., … Nestrasil, I. (2022). Quantitative brain MRI morphology in severe and attenuated forms of mucopolysaccharidosis type I. *Molecular Genetics and Metabolism*, *135*(2), 122–132. https://doi.org/10.1016/j.ymgme.2022.01.001

Kronlage, M., Schwehr, V., Schwarz, D., Godel, T., Heiland, S., Bendszus, M., & Bäumer, P. (2019). Magnetic Resonance Neurography : Normal Values and Demographic Determinants of Nerve Caliber and T2 Relaxometry in 60 healthy individuals. *Clinical Neuroradiology*, *29*(1), 19–26. https://doi.org/10.1007/s00062-017-0633-5

Kullmann, S., Callaghan, M. F., Heni, M., Weiskopf, N., Scheffler, K., Häring, H.-U., Fritsche, A., Veit, R., & Preissl, H. (2016). Specific white matter tissue microstructure changes associated with obesity. *NeuroImage*, *125*, 36–44. https://doi.org/10.1016/j.neuroimage.2015.10.006

Labounek, R., Valošek, J., Horák, T., Svátková, A., Bednařík, P., Vojtíšek, L., Horáková, M., Nestrašil, I., Lenglet, C., Cohen-Adad, J., Bednařík, J., & Hluštík, P. (2020). HARDI-ZOOMit protocol improves specificity to microstructural changes in presymptomatic myelopathy. *Scientific Reports*, *10*(1), 17529. https://doi.org/10.1038/s41598-020-70297-3

Larsson, S. C., Traylor, M., Burgess, S., & Markus, H. S. (2017). Genetically-predicted adult height and Alzheimer's disease. *Journal of Alzheimer's Disease: JAD*, *60*(2), 691–698. https://doi.org/10.3233/JAD-170528

Lema, A., Bishop, C., Malik, O., Mattoscio, M., Ali, R., Nicholas, R., Muraro, P. A., Matthews, P. M., Waldman, A. D., & Newbould, R. D. (2017). A Comparison of Magnetization Transfer Methods to Assess Brain and Cervical Cord Microstructure in Multiple Sclerosis. *Journal of Neuroimaging: Official Journal of the American Society of Neuroimaging*, *27*(2), 221–226. https://doi.org/10.1111/jon.12377

Levitan, I. B., & Kaczmarek, L. K. (2002). *The Neuron: Cell and Molecular Biology*. Oxford University Press. https://play.google.com/store/books/details?id=yTXS_OAkUmcC

Lévy, S., Benhamou, M., Naaman, C., Rainville, P., Callot, V., & Cohen-Adad, J. (2015). White matter atlas of the human spinal cord with estimation of partial volume effect. *NeuroImage*, *119*, 262–271. https://doi.org/10.1016/j.neuroimage.2015.06.040

Lin, H.-Y., Lee, C.-L., Chiu, P. C., Niu, D.-M., Tsai, F.-J., Hwu, W.-L., Lin, S. J., Lin, J.-L., Chang, T.-M., Chuang, C.-K., & Lin, S.-P. (2019). Relationships among Height, Weight, Body Mass Index, and Age in Taiwanese Children with Different Types of Mucopolysaccharidoses. *Diagnostics (Basel, Switzerland)*, *9*(4). https://doi.org/10.3390/diagnostics9040148

Littlejohns, T. J., Holliday, J., Gibson, L. M., Garratt, S., Oesingmann, N., Alfaro-Almagro, F., Bell, J. D., Boultwood, C., Collins, R., Conroy, M. C., Crabtree, N., Doherty, N., Frangi, A. F., Harvey, N. C., Leeson, P., Miller, K. L., Neubauer, S., Petersen, S. E., Sellors, J., … Allen, N. E. (2020). The UK Biobank imaging enhancement of 100,000 participants: rationale, data collection, management and future directions. In *Nature Communications* (Vol. 11, Issue 1). https://doi.org/10.1038/s41467-020-15948-9

Liu, S., Seidlitz, J., Blumenthal, J. D., Clasen, L. S., & Raznahan, A. (2020). Integrative structural, functional,

and transcriptomic analyses of sex-biased brain organization in humans. *Proceedings of the National Academy of Sciences of the United States of America*, *117*(31), 18788–18798. https://doi.org/10.1073/pnas.1919091117

Lopez-Rios, N., Gilbert, K. M., Papp, D., Cereza, G., Foias, A., Rangaprakash, D., May, M. W., Guerin, B., Wald, L. L., Keil, B., Stockmann, J. P., Barry, R. L., & Cohen-Adad, J. (2023). An 8-channel Tx dipole and 20-channel Rx loop coil array for MRI of the cervical spinal cord at 7 Tesla. *NMR in Biomedicine*, *36*(11), e5002. https://doi.org/10.1002/nbm.5002

Lukas, C., Sombekke, M. H., Bellenberg, B., Hahn, H. K., Popescu, V., Bendfeldt, K., Radue, E. W., Gass, A., Borgwardt, S. J., Kappos, L., Naegelin, Y., Knol, D. L., Polman, C. H., Geurts, J. J. G., Barkhof, F., & Vrenken, H. (2013). Relevance of spinal cord abnormalities to clinical disability in multiple sclerosis: MR imaging findings in a large cohort of patients. *Radiology*, *269*(2), 542–552. https://doi.org/10.1148/radiol.13122566

Lv, H., Zeng, N., Li, M., Sun, J., Wu, N., Xu, M., Chen, Q., Zhao, X., Chen, S., Liu, W., Li, X., Zhao, P., Wintermark, M., Hui, Y., Li, J., Wu, S., & Wang, Z. (2024). Association between body mass index and brain health in adults: A 16-year population-based cohort and Mendelian randomization study. *Health Data Science*, *4*, 0087. https://doi.org/10.34133/hds.0087

MacLarnon, A. (1995). The distribution of spinal cord tissues and locomotor adaptation in primates. *Journal of Human Evolution*, *29*(5), 463–482. https://doi.org/10.1006/jhev.1995.1069

MacLarnon, A. (1996a). The evolution of the spinal cord in primates: evidence from the foramen magnum and the vertebral canal. *Journal of Human Evolution*, *30*(2), 121–138. https://doi.org/10.1006/jhev.1996.0009

MacLarnon, A. (1996b). The scaling of gross dimensions of the spinal cord in primates and other species. *Journal of Human Evolution*, *30*(1), 71–87. https://doi.org/10.1006/jhev.1996.0005

Manjón, J. V., & Coupé, P. (2016). VolBrain: An online MRI brain volumetry system. *Frontiers in Neuroinformatics*, *10*, 30. https://doi.org/10.3389/fninf.2016.00030

Martin, A. R., De Leener, B., Cohen-Adad, J., Cadotte, D. W., Kalsi-Ryan, S., Lange, S. F., Tetreault, L., Nouri, A., Crawley, A., Mikulis, D. J., Ginsberg, H., & Fehlings, M. G. (2017). Clinically feasible microstructural MRI to quantify cervical spinal cord tissue injury using DTI, MT, and T2*-weighted imaging: Assessment of normative data and reliability. *AJNR. American Journal of Neuroradiology*, *38*(6), 1257–1265. https://doi.org/10.3174/ajnr.A5163

Martin, A. R., De Leener, B., Cohen-Adad, J., Cadotte, D. W., Nouri, A., Wilson, J. R., Tetreault, L., Crawley, A. P., Mikulis, D. J., Ginsberg, H., & Fehlings, M. G. (2018). Can microstructural MRI detect subclinical tissue injury in subjects with asymptomatic cervical spinal cord compression? A prospective cohort study. *BMJ Open*, *8*(4), e019809. https://doi.org/10.1136/bmjopen-2017-019809

Masuda, H., Mori, M., Hirano, S., Uzawa, A., Uchida, T., Muto, M., Ohtani, R., Aoki, R., & Kuwabara, S. (2022). Silent progression of brain atrophy in aquaporin-4 antibody-positive neuromyelitis optica spectrum disorder. *Journal of Neurology, Neurosurgery, and Psychiatry*, *93*(1), 32–40. https://doi.org/10.1136/jnnp-2021-326386

Miller, K. L., Alfaro-Almagro, F., Bangerter, N. K., Thomas, D. L., Yacoub, E., Xu, J., Bartsch, A. J., Jbabdi, S., Sotiropoulos, S. N., Andersson, J. L. R., Griffanti, L., Douaud, G., Okell, T. W., Weale, P., Dragonu, I., Garratt, S., Hudson, S., Collins, R., Jenkinson, M., … Smith, S. M. (2016). Multimodal population brain imaging in the UK Biobank prospective epidemiological study. *Nature Neuroscience*, *19*(11), 1523–1536. https://doi.org/10.1038/nn.4393

Muschol, N. M., Pape, D., Kossow, K., Ullrich, K., Arash-Kaps, L., Hennermann, J. B., Stücker, R., & Breyer, S. R. (2019). Growth charts for patients with Sanfilippo syndrome (Mucopolysaccharidosis type III). *Orphanet Journal of Rare Diseases*, *14*(1), 93. https://doi.org/10.1186/s13023-019-1065-x

Narvacan, K., Treit, S., Camicioli, R., Martin, W., & Beaulieu, C. (2017). Evolution of deep gray matter volume across the human lifespan. *Human Brain Mapping*, *38*(8), 3771–3790. https://doi.org/10.1002/hbm.23604

Nerland, S., Stokkan, T. S., Jørgensen, K. N., Wortinger, L. A., Richard, G., Beck, D., van der Meer, D., Westlye, L. T., Andreassen, O. A., Agartz, I., & Barth, C. (2022). A comparison of intracranial volume estimation methods and their cross-sectional and longitudinal associations with age. *Human Brain Mapping*, *43*(15), 4620–4639. https://doi.org/10.1002/hbm.25978

Nouri, A., Martin, A. R., Mikulis, D., & Fehlings, M. G. (2016). Magnetic resonance imaging assessment of degenerative cervical myelopathy: a review of structural changes and measurement techniques. *Neurosurgical Focus*, *40*(6), E5. https://doi.org/10.3171/2016.3.focus1667

Nuttall, F. Q. (2015). Body mass index: Obesity, BMI, and health: A critical review. *Nutrition Today*, *50*(3), 117–128. https://doi.org/10.1097/NT.0000000000000092

Okudzhava, L., Heldmann, M., & Münte, T. F. (2022). A systematic review of diffusion tensor imaging studies in obesity. *Obesity Reviews: An Official Journal of the International Association for the Study of Obesity*, *23*(3), e13388. https://doi.org/10.1111/obr.13388

Papinutto, N., Asteggiano, C., Bischof, A., Gundel, T. J., Caverzasi, E., Stern, W. A., Bastianello, S., Hauser, S. L., & Henry, R. G. (2020). Intersubject Variability and Normalization Strategies for Spinal Cord Total Cross-Sectional and Gray Matter Areas. *Journal of Neuroimaging: Official Journal of the American Society of Neuroimaging*, *30*(1), 110–118. https://doi.org/10.1111/jon.12666

Papinutto, N., Schlaeger, R., Panara, V., Zhu, A. H., Caverzasi, E., Stern, W. A., Hauser, S. L., & Henry, R. G. (2015). Age, Gender and Normalization Covariates for Spinal Cord Gray Matter and Total Cross-Sectional Areas at Cervical and Thoracic Levels: A 2D Phase Sensitive Inversion Recovery Imaging Study. In *PLOS ONE* (Vol. 10, Issue 3, p. e0118576). https://doi.org/10.1371/journal.pone.0118576

Patel, M., McCormick, A., Tamaroff, J., Dunn, J., Mitchell, J. A., Lin, K. Y., Farmer, J., Rummey, C., Perlman, S. L., Delatycki, M. B., Wilmot, G. R., Mathews, K. D., Yoon, G., Hoyle, J., Corti, M., Subramony, S. H., Zesiewicz, T., Lynch, D., & McCormack, S. E. (2021). Body Mass Index and Height in the Friedreich Ataxia Clinical Outcome Measures Study. *Neurology. Genetics*, *7*(6), e638. https://doi.org/10.1212/NXG.0000000000000638

Patel, P., Suzuki, Y., Maeda, M., Yasuda, E., Shimada, T., Orii, K. E., Orii, T., & Tomatsu, S. (2014). Growth charts for patients with Hunter syndrome. *Molecular Genetics and Metabolism Reports*, *1*, 5–18. https://doi.org/10.1016/j.ymgmr.2013.10.001

Peters, R. (2006). Ageing and the brain: This article is part of a series on ageing edited by Professor Chris Bulpitt. *Postgraduate Medical Journal*, *82*(964), 84–88. https://doi.org/10.1136/pgmj.2005.036665

Piccolo, L. R., Merz, E. C., He, X., Sowell, E. R., Noble, K. G., & Pediatric Imaging, Neurocognition, Genetics Study. (2016). Age-Related Differences in Cortical Thickness Vary by Socioeconomic Status. *PloS One*, *11*(9), e0162511. https://doi.org/10.1371/journal.pone.0162511

Pierpont, E. I., Bennett, A. M., Schoyer, L., Stronach, B., Anschutz, A., Borrie, S. C., Briggs, B., Burkitt-Wright, E., Castel, P., Cirstea, I. C., Draaisma, F., Ellis, M., Fear, V. S., Frone, M. N., Flex, E., Gelb, B. D., Green, T., Gripp, K. W., Khoshkhoo, S., … Andelfinger, G. (2024). The 8th International RASopathies Symposium: Expanding research and care practice through global collaboration and advocacy. *American Journal of Medical Genetics. Part A*, *194*(4), e63477. https://doi.org/10.1002/ajmg.a.63477

Pisharady, P. K., Eberly, L. E., Cheong, I., Manousakis, G., Guliani, G., Clark, H. B., Bathe, M., Walk, D., & Lenglet, C. (2020). Tract-specific analysis improves sensitivity of spinal cord diffusion MRI to cross-sectional and longitudinal changes in amyotrophic lateral sclerosis. *Communications Biology*, *3*(1), 370. https://doi.org/10.1038/s42003-020-1093-z

Pritschet, L., Taylor, C. M., Cossio, D., Faskowitz, J., Santander, T., Handwerker, D. A., Grotzinger, H., Layher, E., Chrastil, E. R., & Jacobs, E. G. (2024). Neuroanatomical changes observed over the course of a human pregnancy. *Nature Neuroscience*, *27*(11), 2253–2260. https://doi.org/10.1038/s41593-024-01741-0

Provenzale, J. M., Nestrasil, I., Chen, S., Kan, S.-H., Le, S. Q., Jens, J. K., Snella, E. M., Vondrak, K. N., Yee, J. K., Vite, C. H., Elashoff, D., Duan, L., Wang, R. Y., Ellinwood, N. M., Guzman, M. A., Shapiro, E. G., & Dickson, P. I. (2015). Diffusion tensor imaging and myelin composition analysis reveal abnormal myelination in corpus callosum of canine mucopolysaccharidosis I. *Experimental Neurology*, *273*, 1–10. https://doi.org/10.1016/j.expneurol.2015.07.021

Purves, D., Augustine, G. J., Fitzpatrick, D., Katz, L. C., LaMantia, A.-S., McNamara, J. O., & Mark Williams, S. (2001). *Projections from the Cerebellum*. Sinauer Associates. https://www.ncbi.nlm.nih.gov/books/NBK11100/

Querin, G., El Mendili, M. M., Lenglet, T., Delphine, S., Marchand-Pauvert, V., Benali, H., & Pradat, P.-F. (2017). Spinal cord multi-parametric magnetic resonance imaging for survival prediction in amyotrophic lateral sclerosis. *European Journal of Neurology: The Official Journal of the European Federation of Neurological Societies*, *24*(8), 1040–1046. https://onlinelibrary.wiley.com/doi/abs/10.1111/ene.13329

Reading, S. A. J., Yassa, M. A., Bakker, A., Dziorny, A. C., Gourley, L. M., Yallapragada, V., Rosenblatt, A., Margolis, R. L., Aylward, E. H., Brandt, J., Mori, S., van Zijl, P., Bassett, S. S., & Ross, C. A. (2005). Regional white matter change in pre-symptomatic Huntington's disease: a diffusion tensor imaging study. *Psychiatry Research*, *140*(1), 55–62. https://doi.org/10.1016/j.pscychresns.2005.05.011

Rezende, T. J. R., Adanyeguh, I. M., Arrigoni, F., Bender, B., Cendes, F., Corben, L. A., Deistung, A., Delatycki, M., Dogan, I., Egan, G. F., Göricke, S. L., Georgiou-Karistianis, N., Henry, P.-G., Hutter, D., Jahanshad, N., Joers, J. M., Lenglet, C., Lindig, T., Martinez, A. R. M., … França, M. C., Jr. (2023). Progressive spinal cord degeneration in Friedreich's ataxia: Results from ENIGMA-ataxia. *Movement Disorders: Official*

Journal of the Movement Disorder Society, *38*(1), 45–56. https://doi.org/10.1002/mds.29261

Ringman, J. M., O'Neill, J., Geschwind, D., Medina, L., Apostolova, L. G., Rodriguez, Y., Schaffer, B., Varpetian, A., Tseng, B., Ortiz, F., Fitten, J., Cummings, J. L., & Bartzokis, G. (2007). Diffusion tensor imaging in preclinical and presymptomatic carriers of familial Alzheimer's disease mutations. *Brain: A Journal of Neurology*, *130*(Pt 7), 1767–1776. https://doi.org/10.1093/brain/awm102

Rosano, C., Kuller, L. H., Chung, H., Arnold, A. M., Longstreth, W. T., Jr, & Newman, A. B. (2005). Subclinical brain magnetic resonance imaging abnormalities predict physical functional decline in high-functioning older adults. *Journal of the American Geriatrics Society*, *53*(4), 649–654. https://doi.org/10.1111/j.1532-5415.2005.53214.x

Rosano, C., Sigurdsson, S., Siggeirsdottir, K., Phillips, C. L., Garcia, M., Jonsson, P. V., Eiriksdottir, G., Newman, A. B., Harris, T. B., van Buchem, M. A., Gudnason, V., & Launer, L. J. (2010). Magnetization transfer imaging, white matter hyperintensities, brain atrophy and slower gait in older men and women. *Neurobiology of Aging*, *31*(7), 1197–1204. https://doi.org/10.1016/j.neurobiolaging.2008.08.004

Rosas, H. D., Tuch, D. S., Hevelone, N. D., Zaleta, A. K., Vangel, M., Hersch, S. M., & Salat, D. H. (2006). Diffusion tensor imaging in presymptomatic and early Huntington's disease: Selective white matter pathology and its relationship to clinical measures. *Movement Disorders: Official Journal of the Movement Disorder Society*, *21*(9), 1317–1325. https://doi.org/10.1002/mds.20979

Rovira, A., Grivé, E., Pedraza, S., Rovira, A., & Alonso, J. (2001). Magnetization transfer ratio values and proton MR spectroscopy of normal-appearing cerebral white matter in patients with liver cirrhosis. *AJNR. American Journal of Neuroradiology*, *22*(6), 1137–1142. https://www.ncbi.nlm.nih.gov/pubmed/11415910

Rushton, W. A. H. (1951). A theory of the effects of fibre size in medullated nerve. *The Journal of Physiology*, *115*(1), 101–122. https://doi.org/10.1113/jphysiol.1951.sp004655

Saliani, A., Perraud, B., Duval, T., Stikov, N., Rossignol, S., & Cohen-Adad, J. (2017). Axon and Myelin Morphology in Animal and Human Spinal Cord. *Frontiers in Neuroanatomy*, *11*, 129. https://doi.org/10.3389/fnana.2017.00129

Schmierer, K., Scaravilli, F., Altmann, D. R., Barker, G. J., & Miller, D. H. (2004). Magnetization transfer ratio and myelin in postmortem multiple sclerosis brain. *Annals of Neurology*, *56*(3), 407–415. https://doi.org/10.1002/ana.20202

Seitz, J., Bühren, K., von Polier, G. G., Heussen, N., Herpertz-Dahlmann, B., & Konrad, K. (2014). Morphological changes in the brain of acutely ill and weight-recovered patients with anorexia nervosa. A meta-analysis and qualitative review. *Zeitschrift Fur Kinder- Und Jugendpsychiatrie Und Psychotherapie*, *42*(1), 7–17; quiz 17–18. https://doi.org/10.1024/1422-4917/a000265

Smith, S. M., Zhang, Y., Jenkinson, M., Chen, J., Matthews, P. M., Federico, A., & De Stefano, N. (2002). Accurate, robust, and automated longitudinal and cross-sectional brain change analysis. *NeuroImage*, *17*(1), 479–489. https://doi.org/10.1006/nimg.2002.1040

Sowell, E. R., Peterson, B. S., Kan, E., Woods, R. P., Yoshii, J., Bansal, R., Xu, D., Zhu, H., Thompson, P. M., & Toga, A. W. (2007). Sex differences in cortical thickness mapped in 176 healthy individuals between 7 and 87 years of age. *Cerebral Cortex* , *17*(7), 1550–1560. https://doi.org/10.1093/cercor/bhl066

Susuki, K. (2010). Myelin: a specialized membrane for cell communication. *Nature Education*, *3*(9), 59.

Tamnes, C. K., Ostby, Y., Fjell, A. M., Westlye, L. T., Due-Tønnessen, P., & Walhovd, K. B. (2010). Brain maturation in adolescence and young adulthood: regional age-related changes in cortical thickness and white matter volume and microstructure. *Cerebral Cortex* , *20*(3), 534–548. https://doi.org/10.1093/cercor/bhp118

Thambisetty, M., Wan, J., Carass, A., An, Y., Prince, J. L., & Resnick, S. M. (2010). Longitudinal changes in cortical thickness associated with normal aging. In *NeuroImage* (Vol. 52, Issue 4, pp. 1215–1223). https://doi.org/10.1016/j.neuroimage.2010.04.258

Valošek, J., Bédard, S., Keřkovský, M., Rohan, T., & Cohen-Adad, J. (2024). A database of the healthy human spinal cord morphometry in the PAM50 template space. *Imaging Neuroscience*, *2*, 1–15. https://doi.org/10.1162/imag_a_00075

Valošek, J., Labounek, R., Horák, T., Horáková, M., Bednařík, P., Keřkovský, M., Kočica, J., Rohan, T., Lenglet, C., Cohen‐Adad, J., Hluštík, P., Vlčková, E., Kadaňka, Z., Bednařík, J., & Svatkova, A. (2021). Diffusion MRI reveals tract‐specific microstructural correlates of electrophysiological impairments in non‐myelopathic and myelopathic spinal cord compression. *European Journal of Neurology: The Official Journal of the European Federation of Neurological Societies*, *28*, 3784–3797. https://doi.org/10.1111/ene.15027

van de Stadt, S. I. W., van Ballegoij, W. J. C., Labounek, R., Huffnagel, I. C., Kemp, S., Nestrasil, I., & Engelen,

M. (2020). Spinal cord atrophy as a measure of severity of myelopathy in adrenoleukodystrophy. *Journal of Inherited Metabolic Disease*, *43*(4), 852–860. https://doi.org/10.1002/jimd.12226

Veraart, J., Nunes, D., Rudrapatna, U., Fieremans, E., Jones, D. K., Novikov, D. S., & Shemesh, N. (2020). Noninvasive quantification of axon radii using diffusion MRI. *eLife*, *9*, e49855. https://doi.org/10.7554/eLife.49855

Voevodskaya, O., Simmons, A., Nordenskjöld, R., Kullberg, J., Ahlström, H., Lind, L., Wahlund, L.-O., Larsson, E.-M., Westman, E., & Alzheimer's Disease Neuroimaging Initiative. (2014). The effects of intracranial volume adjustment approaches on multiple regional MRI volumes in healthy aging and Alzheimer's disease. *Frontiers in Aging Neuroscience*, *6*, 264. https://doi.org/10.3389/fnagi.2014.00264

Vuoksimaa, E., Panizzon, M. S., Franz, C. E., Fennema-Notestine, C., Hagler, D. J., Jr, Lyons, M. J., Dale, A. M., & Kremen, W. S. (2018). Brain structure mediates the association between height and cognitive ability. *Brain Structure & Function*, *223*(7), 3487–3494. https://doi.org/10.1007/s00429-018-1675-4

Wade, A., Jacobs, P., & Morton, A. J. (2008). Atrophy and degeneration in sciatic nerve of presymptomatic mice carrying the Huntington's disease mutation. *Brain Research*, *1188*, 61–68. https://doi.org/10.1016/j.brainres.2007.06.059

Wang, J., Hill-Jarrett, T., Buto, P., Pederson, A., Sims, K. D., Zimmerman, S. C., DeVost, M. A., Ferguson, E., Lacar, B., Yang, Y., Choi, M., Caunca, M. R., La Joie, R., Chen, R., Glymour, M. M., & Ackley, S. F. (2024). Comparison of approaches to control for intracranial volume in research on the association of brain volumes with cognitive outcomes. *Human Brain Mapping*, *45*(4), e26633. https://doi.org/10.1002/hbm.26633

Ward, M. A., Carlsson, C. M., Trivedi, M. A., Sager, M. A., & Johnson, S. C. (2005). The effect of body mass index on global brain volume in middle-aged adults: a cross sectional study. *BMC Neurology*, *5*(1), 23. https://doi.org/10.1186/1471-2377-5-23

Weitzenkamp, D. A., Jones, R. H., Whiteneck, G. G., & Young, D. A. (2001). Ageing with spinal cord injury: cross-sectional and longitudinal effects. *Spinal Cord*, *39*(6), 301–309. https://doi.org/10.1038/sj.sc.3101146

West, R. K., Livny, A., Ravona-Springer, R., Bendlin, B. B., Heymann, A., Leroith, D., Liu, X., Lin, H.-M., Hochner, H., Friedlander, Y., Ganmore, I., Tirosh, A., & Schnaider Beeri, M. (2020). Higher BMI is associated with smaller regional brain volume in older adults with type 2 diabetes. *Diabetologia*, *63*(11), 2446–2451. https://doi.org/10.1007/s00125-020-05264-8

Whitwell, J. L., Crum, W. R., Watt, H. C., & Fox, N. C. (2001). Normalization of cerebral volumes by use of intracranial volume: implications for longitudinal quantitative MR imaging. *AJNR. American Journal of Neuroradiology*, *22*(8), 1483–1489. https://www.ncbi.nlm.nih.gov/pubmed/11559495

Willerman, L., Schultz, R., Neal Rutledge, J., & Bigler, E. D. (1991). In vivo brain size and intelligence. *Intelligence*, *15*(2), 223–228. https://doi.org/10.1016/0160-2896(91)90031-8

Woo, A., Botta, A., Shi, S. S. W., Paus, T., & Pausova, Z. (2022). Obesity-Related Neuroinflammation: Magnetic Resonance and Microscopy Imaging of the Brain. *International Journal of Molecular Sciences*, *23*(15). https://doi.org/10.3390/ijms23158790

Xie, S., Xiao, J. X., Wang, Y. H., Wu, H. K., Gong, G. L., & Jiang, X. X. (2005). Evaluation of bilateral cingulum with tractography in patients with Alzheimer's disease. *Neuroreport*, *16*(12), 1275–1278. https://doi.org/10.1097/01.wnr.0000174061.41897.ee

Yund, B., Rudser, K., Ahmed, A., Kovac, V., Nestrasil, I., Raiman, J., Mamak, E., Harmatz, P., Steiner, R., Lau, H., Vekaria, P., Wozniak, J. R., Lim, K. O., Delaney, K., Whitley, C., & Shapiro, E. G. (2015). Cognitive, medical, and neuroimaging characteristics of attenuated mucopolysaccharidosis type II. *Molecular Genetics and Metabolism*, *114*(2), 170–177. https://doi.org/10.1016/j.ymgme.2014.12.299

Yushkevich, P. A., Piven, J., Hazlett, H. C., Smith, R. G., Ho, S., Gee, J. C., & Gerig, G. (2006). User-guided 3D active contour segmentation of anatomical structures: significantly improved efficiency and reliability. *NeuroImage*, *31*(3), 1116–1128. https://doi.org/10.1016/j.neuroimage.2006.01.015

Zalc, B. (2006). The acquisition of myelin: a success story. *Novartis Foundation Symposium*, *276*, 15–21; discussion 21–25, 54–57, 275–281. https://doi.org/10.1002/9780470032244.ch3

Zalc, B. (2016). The acquisition of myelin: An evolutionary perspective. *Brain Research*, *1641*(Pt A), 4–10. https://doi.org/10.1016/j.brainres.2015.09.005

Zhang, C., Zhou, M., Shiraishi, N., & Goto, N. (1996). Morphometric Analysis of Age-related Changes in the Human Cervical Spinal Cord. *The Showa University Journal of Medical Sciences*, *8*(1), 29–38. https://doi.org/10.15369/sujms1989.8.29

Zhou, M., Goto, N., Zhang, C., & Tang, W. (1996). Aging process of the human lumbar spinal cord: A

morphometric analysis. *Neuropathology: Official Journal of the Japanese Society of Neuropathology*, *16*(2), 106–111. https://doi.org/10.1111/j.1440-1789.1996.tb00164.x

Zyoud, T. Y. T., Abdul Rashid, S. N., Suppiah, S., Mahmud, R., Kabeer, A., Abd Manaf, R., & Abdul Rahim, E. (2020). Estimation of body height from spinal length measurements using post-mortem computed tomographic images. *The Malaysian Journal of Pathology*, *42*(3), 423–431. https://www.ncbi.nlm.nih.gov/pubmed/33361724